

Dynamic Contrast-Enhanced T₁-Weighted MR Imaging: Theory, Quantitative Aspects, and Practical Implementation

Henrik Bo Wiberg Larsson, MD, PhD, and Thomas Fritz Hansen, MD

Introduction

Dynamic contrast-enhanced T₁-weighted MRI (DCE-MRI) is relatively easy to integrate in a conventional MRI setup, it is cheap, and it has the potential to provide important physiologic parameters. Large interest has focused on determination of the leakage, also called the permeability, of the capillary membranes. The reason is that the permeability can be associated with changes in the vascular structure seen in malign transformed tissue and in tissue inflammation. The reason why the DCE-MRI has this potential is the size of the contrast agent (CA) molecules we are using. Typically, MRI CA agents are not freely diffusible in tissue, and the capillary membrane normally imposes restriction of diffusivity through the capillary membrane in normal tissue. In the brain, the normal blood–brain barrier (BBB) is nearly impermeable for conventional MRI CA, but the barrier breaks down in a number of diseases such as acute multiple sclerosis, inflammation, tumors, stroke, and possible dementia and epilepsy.^{1,2} Permeability is expressed as the permeability–surface area (PS) product, signifying that not only the permeability but also the available capillary surface area is determinant for the leakage. The PS product is ideally defined from a two-chamber experiment, the chamber having an initial concentration of C₁ and C₂ and J denoting the initial flux, that is, number of molecules moving from the first compartment to the second compartment per time unit. The relationship is

$$J_{1 \rightarrow 2} = -PS(C_2 - C_1) \quad (1)$$

Note the transport is sign sensitive. The equation implies a first-order transport, that is, the flux out of a compartment is proportional to the concentration in that compartment, which is a reasonable assumption, because MRI CA are inert molecules and do not react with specific receptors. However, if the transport over the membrane is governed by a saturable transport system, the Michaelis-Menten kinetics is appropriate. This topic is outside the scope of this presentation. Using conventional MR CA, transport over the capillary membrane is driven by the concentration difference over the membrane as described by the equation. But this is not the whole story, because the blood flow through the capillary (the perfusion) will modify the actual flux over the membrane in a subtle way. Intuitively, the higher velocity of the blood through the capillary, the less likely is a passage over the capillary membrane. It turns out that the determining factor is the ratio PS/F, where

F denotes the flow through the capillary. The dimension of the PS and F is mL/min or corresponding derivatives. The relationship can be derived based on the following considerations: imaging a single capillary of length L and with radius R and having a specific PS product for the specific CA we are using. The flow is F, and the CA concentration at the inlet and outlet of the capillary is C_{in} and C_o, respectively (see Fig. 8.1). In order to simplify matters, these concentrations are constant in time, and we assume that the extravascular concentration is so small that it can be ignored, which also means no return to the blood, once the CA molecules have left the blood over the membrane. These assumptions can easily be modified later if needed and will not change the basic principle we are aiming at. The loss of CA from a short-segment dx centered at position x along the capillary using Eq. (1) is

$$dJ = -\frac{dS}{S} PS(C_e - C_p(x)) = \frac{2\pi r dx}{2\pi r L} PS C_p(x)$$

The CA change inside the capillary over this short segment where the concentrations in a thin layer at the entrance and exit of the short segment are C(x₁) and C(x₂), respectively, is

$$dJ = -F(C(x_2) - C(x_1)) = -F dC(x)$$

Combining and integrate these equations gives

$$\int_{C_{in}}^{C_o} \frac{dC(x)}{C(x)} = -\int_0^L \frac{PS}{LF} dx \Leftrightarrow \ln \frac{C_o}{C_{in}} = -\frac{PS}{F} \Leftrightarrow C_o = C_{in} \exp\left(-\frac{PS}{F}\right) \quad (2)$$

Thus, the concentration at the outlet becomes smaller when the PS product is large relative to F and vice versa, verifying our initial intuition. In the same setup, we can define the extraction fraction as the ratio of the amount taken up by the tissue per unit time to the total amount entering the tissue per unit time:

$$E \equiv \frac{FC_{in} - FC_o}{FC_o} = \frac{C_{in} - C_o}{C_{in}} = 1 - \exp\left(-\frac{PS}{F}\right) \quad (3)$$

Renkin and Crone originally developed these equations.^{3,4} A freely diffusible CA for which PS/F is very large has an extraction of nearly one and is called a flow-limited tracer, because the amount

2 Perfusion Imaging in Clinical Practice

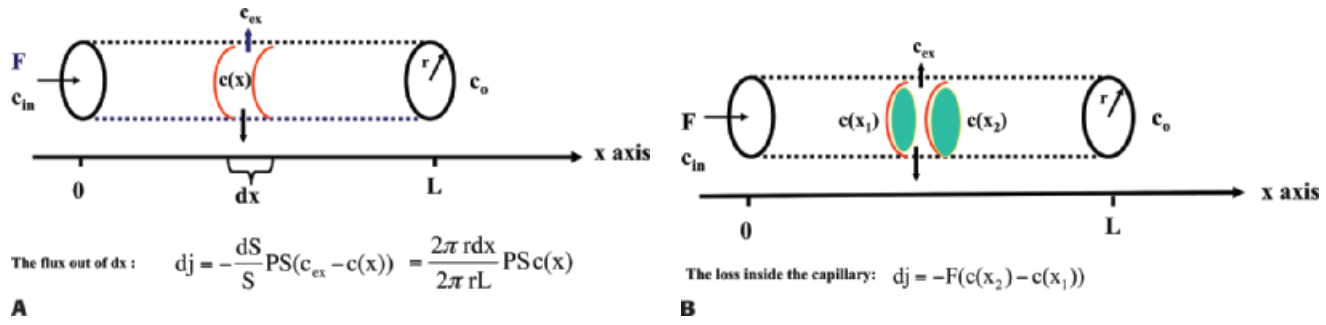


Figure 8-1. The single-unit capillary model used to derive the Crone and Renkin equation. Here, concentrations are only a function of position. Time dependence can be incorporated as well.

in tissue is determined by flow. If the CA is more or less confined to the vascular space, because it cannot easily diffuse over the capillary membrane, then PS/F is small and the extraction fraction approach zero. We then talk about a diffusion-limited CA, because the amount in the extravascular space is determined by the PS product. Note that the amount in the vascular space is of course determined by the delivery of the flowing blood entering the tissue. Because of the flow, Eq. (1) does not really describe the transport adequately. The transport is still linear meaning that the actual flux is proportional to the vascular concentration keeping F and PS the same. In order to deal with this situation, we define the clearance as the amount taken up by the tissue per unit time normalized to a reference concentration:

$$K_1 = \frac{J_{tis}}{C_{ref}} = \frac{FC_{in} - FC_o}{C_{ref}}$$

The dimension of the clearance is then volume per unit time. In words, the clearance is a (fictive) flow and is a measure of the volume of the reference solution containing the amount of the CA taken up or cleared by the tissue per unit time. Often, it is convenient to choose the reference concentration as the concentration of the CA at the inlet. In this case, we get

$$K_1 = \frac{J_{tis}}{C_{in}} = \frac{FC_{in} - FC_o}{C_{in}} = FE \quad (4)$$

and Eq. (1) can be replaced with

$$J_{1 \rightarrow 2} = K_1 C_1 - PS C_2$$

In order not to deal with too many physiologic constants, the last equation is replaced with

$$J_{1 \rightarrow 2} = K_1 C_1 - K_1 C_2$$

using the argument of a membrane transport symmetry, although this may not be strictly correct. Note that K_1 approach F for E going towards 1 for a free diffusible CA (i.e., a flow-limited CA or tracer), while K_1 approaches the PS product for PS/F going towards zero (i.e., a diffusion-limited CA or tracer):

$$K_1 = FE = F \left(1 - \exp\left(-\frac{PS}{F}\right) \right) \approx F - F \left(1 - \frac{PS}{F} \right) = PS$$

It is often convenient to normalize flux, PS product, F , and K_1 to the tissue mass M_t or tissue volume V_t . In the following, relevant capital letters refer to no normalization, while small letters refer to a normalized metric, for example, F is in mL/min, while f is in mL blood/100 mL tissue/min. Strictly, this implies a dimension of

f as 1/min, but it is important to keep the definition in mind. The choice between volume and mass is somewhat arbitrary, but strictly volume V_t and mass M_t are related as $M_t = \rho V_t$, where ρ is the tissue density, close to 1 g/mL.

DCE-MRI also allows determination of various compartment volumes, as the blood volume where V_p denotes the plasma volume, V_b denotes full blood volume, V_e denotes extravascular extracellular volume, and V_{tis} denotes extravascular intracellular tissue volume. Thus, $V_b + V_e + V_{tis} = V_t$, and $V_b/V_t + V_e/V_t + V_{tis}/V_t = v_b + v_e + v_{tis} = 1$, where, for example, v_e either is a fractional volume or has the dimension mL/100 mL or mL/100 g. The relationship between V_b and V_p is given as $V_p = V_b(1 - Hct_{sv})$, where Hct_{sv} is the small vessel hematocrit. More generally, in a given context, we talk about the volume of distribution (V_d) defined as $V_d = Q_t/C_{ref}$ where Q_t is the number of CA molecules in a piece of tissue and C_{ref} is the concentration of a reference solution of the CA, for example, plasma concentration. Ideally, V_d is defined in a situation where equilibration between a piece of tissue and the reference solution has been established. In words, V_d express the volume of the reference solution, which contains an amount equivalent to the amount in the tissue. If we normalize with the mass or volume of the tissue, we get the partition coefficient

$$\lambda = \frac{V_d}{M_t} = \frac{Q_t}{M_t C_{ref}} = \frac{C_t}{C_{ref}} [\text{mL/g}] \quad (5)$$

or

$$\lambda = \frac{V_d}{V_t} = \frac{Q_t}{V_t C_{ref}} = \frac{C_t}{C_{ref}} [\text{mL/mL}]$$

Note that the tissue concentration is then defined as $C_t = Q_t/V_t$ or $C_t = Q_t/M_t$.

DCE-MRI can also be used for assessing tissue perfusion, for example, myocardial perfusion,^{5,6} and lately, it has been shown that when using a high scanner field strength of 3 T, brain perfusion can also be measured by DCE-MRI.^{7,8} Tissue perfusion is vital for normal functionality of the tissue, and lack of adequate tissue perfusion in various organs is the cause of many diseases, and probably more than 50% of all human deaths is directly caused by lack of perfusion, creating tissue starvation, hypoxia, and infarction. In that perspective, it is remarkable that the methodology of perfusion measurement is still a very dynamic research area, and many perfusion methods are based on Kety's pioneering work more than 60 years ago.^{9,10} All perfusion methods have advantages and disadvantages with regard to accuracy, precision, invasiveness, and expensiveness. Accuracy is not necessarily the ultimate goal, but the applicability in clinical decision making may be more relevant.

Tissue perfusion (f) is ideally defined as the volume of blood that enters a distinct part of the vascular system such as the capillaries in one unit of tissue mass (or volume) per unit time. The dimension is therefore mL blood/100 mL tissue/min, which is equal with 1/min. Often, the dimension mL blood/100 g tissue/min is used and reminisces earlier studies of perfusion based on in vitro studies, where perfusion was normalized to mass of tissue. Keeping the older terminology helps keeping the correct interpretation of perfusion, which may become blurred if using 1/min. Because 1 mL of tissue nearly has a mass of 1 g, the number is unchanged.

Determination of perfusion, permeability, and distribution volumes is based on a mathematical framework, the tracer kinetic theory, which in essence are equations describing the mass balance, keeping track of the transport of the CA as a function of time.

Basic Tracer Kinetic Theory

The fundamental equation relating tissue concentration as a function of time, $C_t(t)$, the arterial concentration as a function of time, $C_a(t)$, perfusion f , and the residue impulse response function, RIF(t), is¹¹

$$C_t(t) = C_a(t) \otimes f \text{RIF}(t) = f \int_0^t C_a(\tau) \text{RIF}(t - \tau) d\tau \quad (6)$$

The residue impulse response function is defined as the CA fraction remaining in the tissue, after a brief injected bolus, in principle as a $\delta(t)$ function, directly into the tissue (or voxel), as a function of time. Thus, RIF is dimensionless, and because the entire bolus by definition is injection at time zero, the first function value will be one: $\text{RIF}(0) = 1$. If the entire bolus has a minimum transit time through the tissue (the voxel), of several seconds, then the RIF holds a function value of one until some of the CA molecules begin to leave the tissue in focus. From now on, the RIF will show a monotone decrease until it becomes zero: the entire bolus has left the tissue, or if it happens that a fraction becomes bound irreversibly to the tissue, the RIF ends at a corresponding value, that is, the fraction that remains in the tissue infinitely; this value may be related to the extraction fraction (if back-diffusion does not occur). The assumption related to this equation is that the system is linear: Doubling the dose or concentration, $C_a(t)$, results in a doubling of $C_t(t)$ (f remains the same as well as the RIF), and a delayed input of “ a ” seconds, $C_a(t - a)$, will result in a delayed output ($C_t(t - a)$) and that the CA is not being produced or metabolized inside the tissue. Such a system is called a linear and time-invariant system. This is correct for many of the MRI CA we are using. However, one important additional point is that the CA has to be equally “visible” irrespective of the location of CA, be it in the plasma, the interstitial space, or intracellularly. Due to the fact that MRI CA acts by changing the longitudinal relaxation rate, R_1 , of adjacent water protons corresponding to the first hydration layer, the ability of water diffusion around the paramagnetic core of the CA can influence the level of visibility of the CA. As an example, if the CA becomes confined in a small compartment, without sufficient water exchange, then the CA loses its effect, because complete relaxation of the compartment is finite and therefore becomes invisible, that is, additional CA is without effect (see later).

Under these assumptions of linearity, ignoring the issue of water exchange, the convolution equation can be derived based on the following considerations. Imaging a short bolus $Q_{in}(0) = FC_a(0) dt = V_f C_a(0) dt$ enters a tissue volume (V_t) at time zero. Using the definition of the RIF, the tissue “response” is simply

$$Q_t(t) = V_t f C_a(0) \Delta t \text{RIF}(t)$$

If an additional input enters the tissue volume at a later time point, τ , the tissue response from this input is again

$$Q_t(t) = V_t f C_a(\tau) \Delta t \text{RIF}(t - \tau)$$

Note the time shift of τ seconds of the RIF to the right. The total tissue response is the sum of all tissue response functions. Generally, if we imagine that the entire arterial input function is composed of short inputs (δ -functions), entering as a continuous function of τ (substituting Δt with $d\tau$), and the tissue response is linear in the input, the total tissue response at time t will be the sum of all the tissue impulse responses corresponding to each τ , and we get

$$Q_t(t) / V_t = C_t(t) = C_a(t) \otimes f \text{RIF}(t) = f \int_0^t C_a(\tau) \text{RIF}(t - \tau) d\tau$$

Tissue concentration is here defined as the total amount of CA molecules per unit volume of tissue (or unit mass of tissue).

The integration of two functions as in Eq. (6) is called a convolution integral and is described from an operational point of view in Figure 8.2.

It is remarkable that Eq. (6), under the above-mentioned restriction, is always correct. Obviously, the goal is to find the perfusion f and the RIF(t). The physiologic interpretation of the RIF(t) is that this function describes the destiny of the contrast molecule inside the tissue. The RIF(t) is related to the distribution of transit times through the tissue: $h(t)$. In words, $h(t)$ is the fraction of the CA, which leaves the tissue at time t , per unit time, after a bolus injection:

$$h(t) = \frac{dN(t)}{N_0 dt}$$

where $dN(t)$ is the number of CA molecules leaving the tissue at time t in the time interval dt and N_0 is the entire bolus. Therefore, integrating over time in a time interval will give the fraction having left the tissue volume in that time interval, after a bolus injection. Specifically, in the time interval from zero (bolus injection) to time t_1 , the fraction having left the tissue is

$$\int_0^{t_1} h(t) dt = \frac{1}{N_0} \int_0^{t_1} dN(t) = \frac{1}{N_0} [N(t)]_0^{t_1} = \frac{N(t_1) - N(0)}{N_0} = \frac{N(t_1)}{N_0}$$

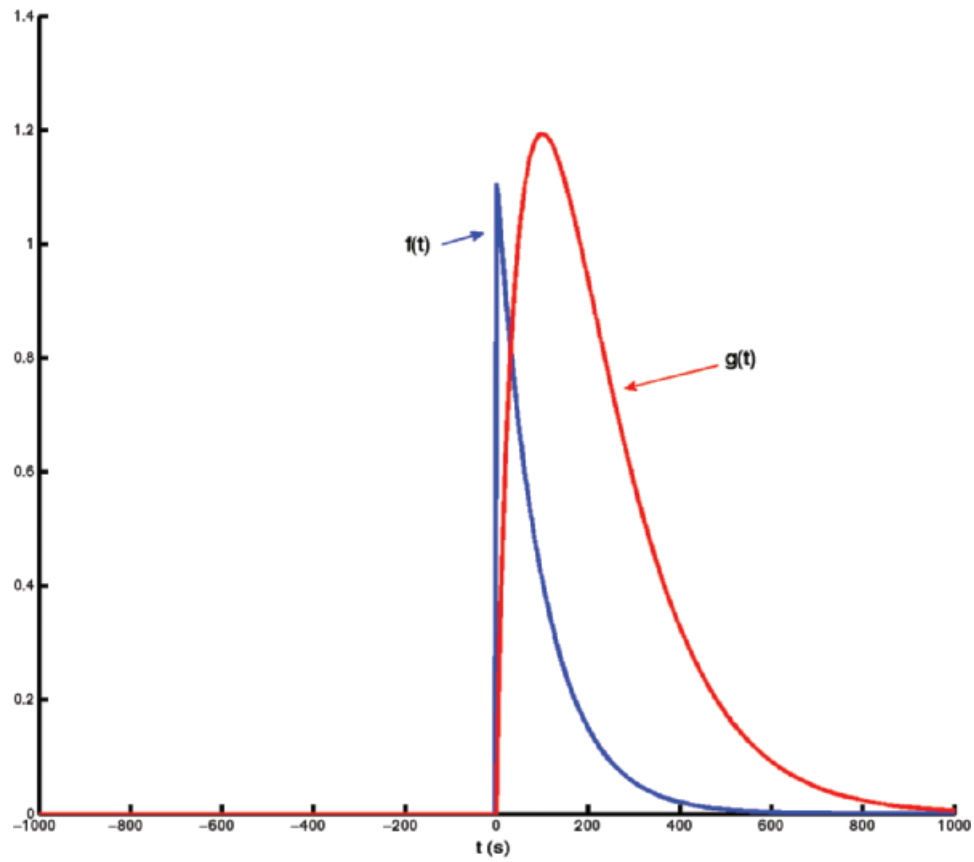
Note $N(0) = 0$: nothing has left the tissue at time zero. The fraction remaining in the tissue at time t_1 is then

$$\frac{N_0 - N(t_1)}{N_0} = 1 - \int_0^{t_1} h(t) dt = \text{RIF}(t_1)$$

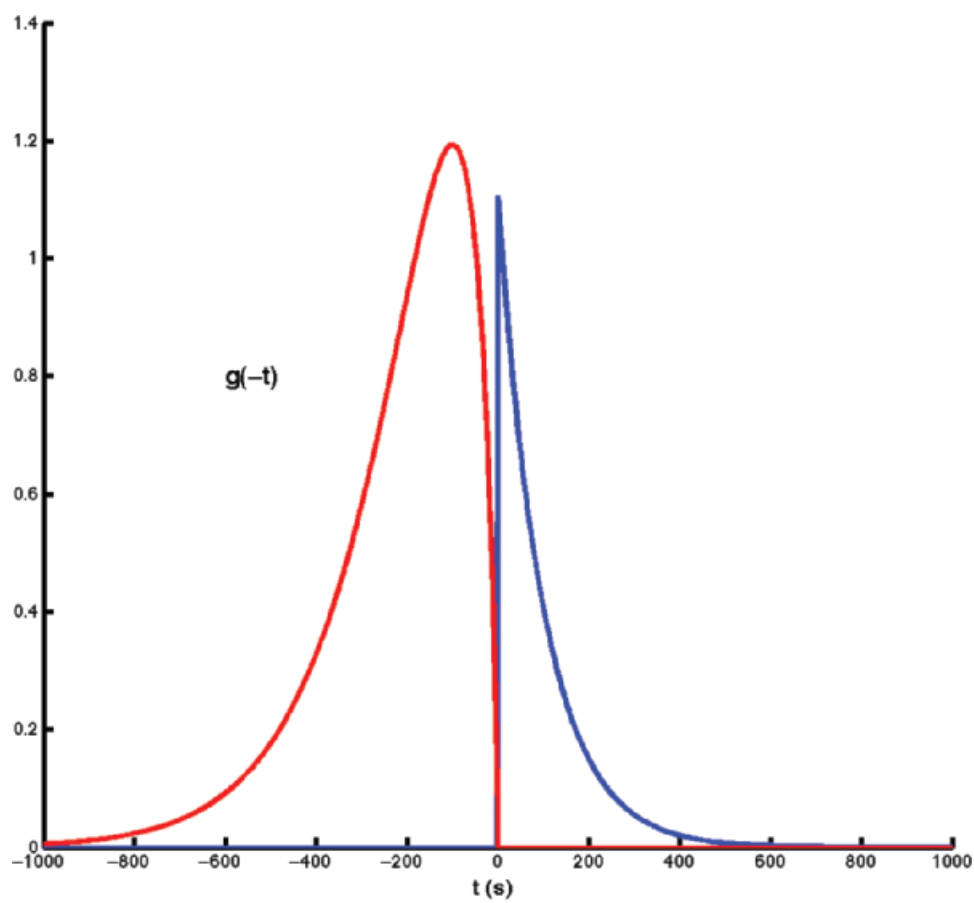
$h(t)$ is similar to a probability density function, known from statistic, and the expectation value of the time weighted distribution is the typical transit time, the mean transit time MTT, and is given as

$$\begin{aligned} \text{MTT} &= \int_0^{\infty} t h(t) dt = - \int_0^{\infty} t \frac{d\text{RIF}(t)}{dt} dt \\ &= - [t \text{RIF}(t)]_0^{\infty} + \int_0^{\infty} \text{RIF}(t) dt = \int_0^{\infty} \text{RIF}(t) dt \end{aligned}$$

where we have used partial integration. Here, we assume that the RIF will be zero after sufficiently long time, that is, all CA molecules will leave the tissue eventually. Thus, MTT can be estimated either from the frequency function, $h(t)$, or from the RIF(t). In Figure 8.3, $h(t)$ is modeled as a gamma-variate function, and the corresponding RIF(t) and $1 - \text{RIF}(t)$ are also shown.

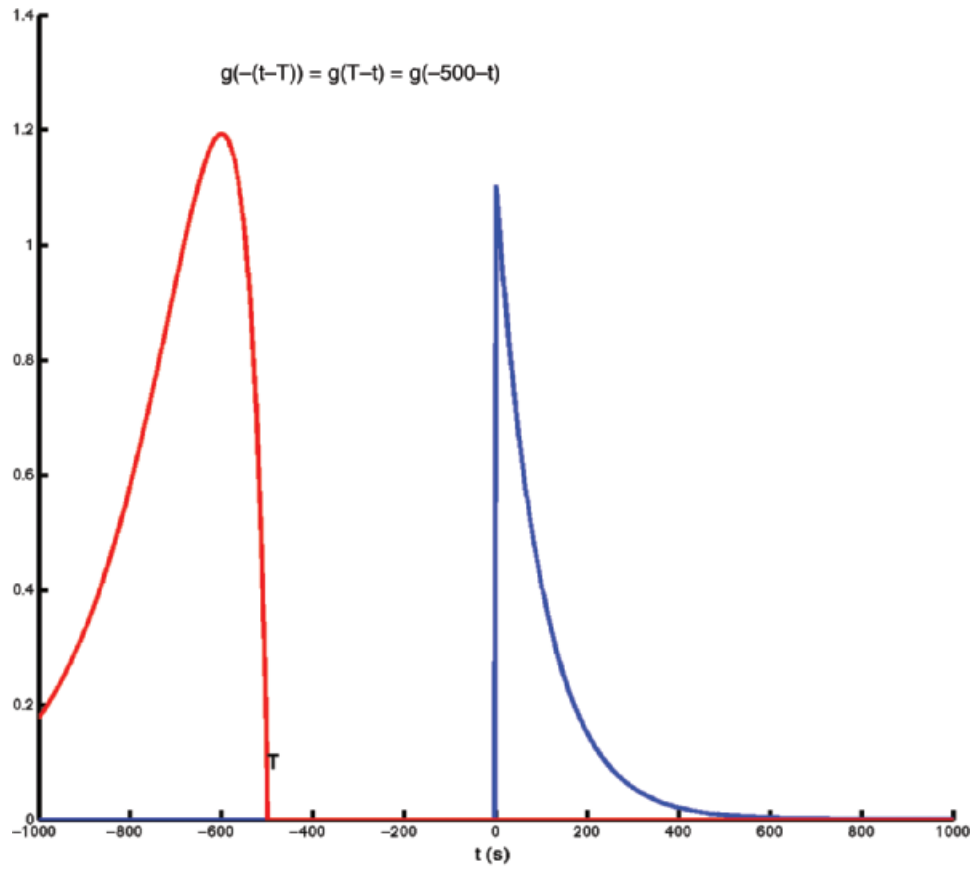


A

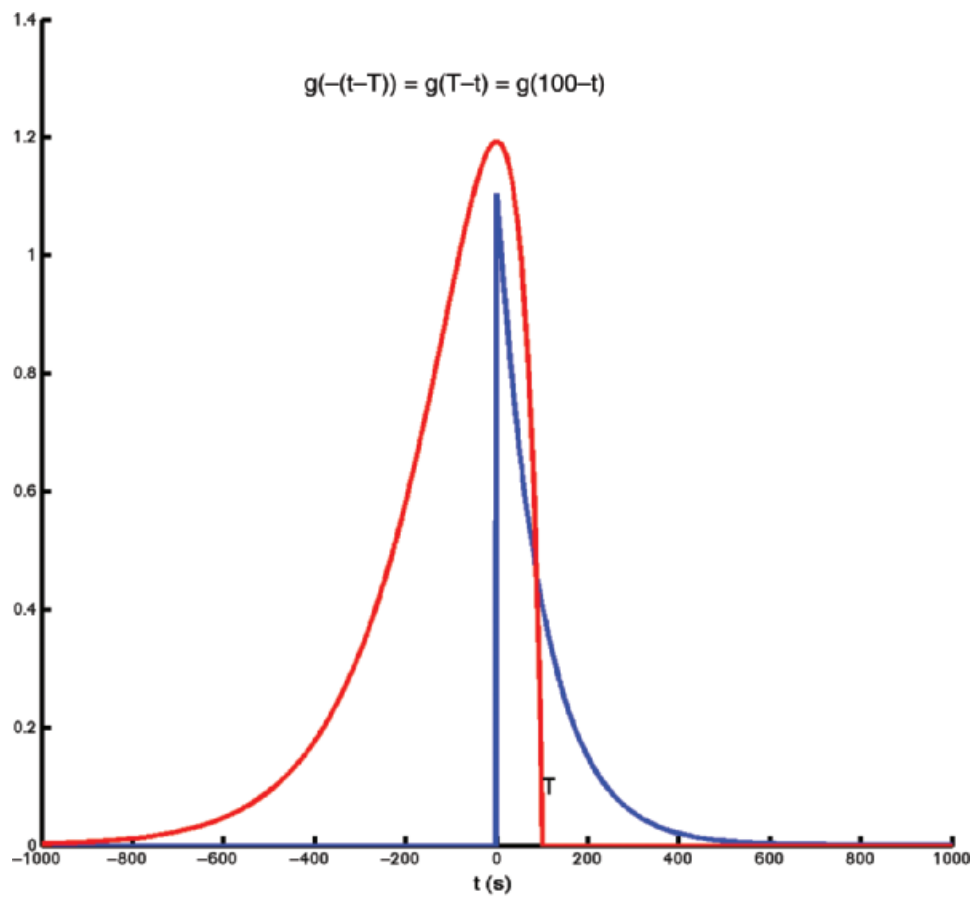


B

Figure 8-2. A: Convolution of two functions $f(t)$ and $g(t)$; the order of the functions is interchangeable. **B:** One of the functions is reflected by changing the sign of the argument, $g(-t)$.



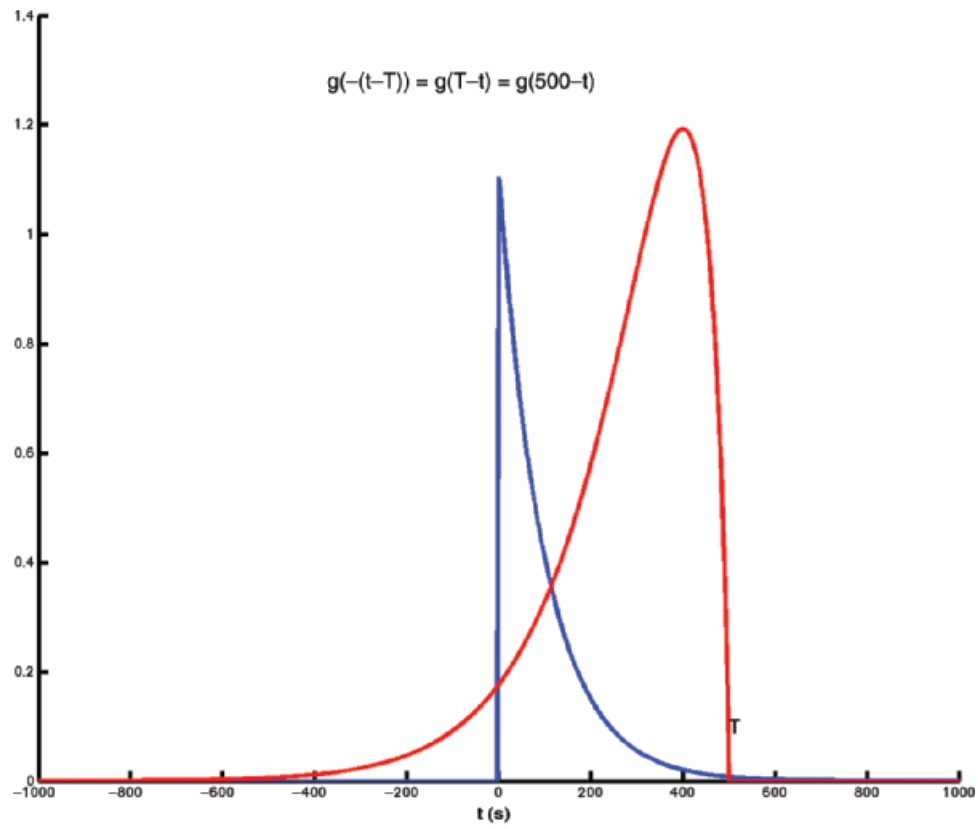
C



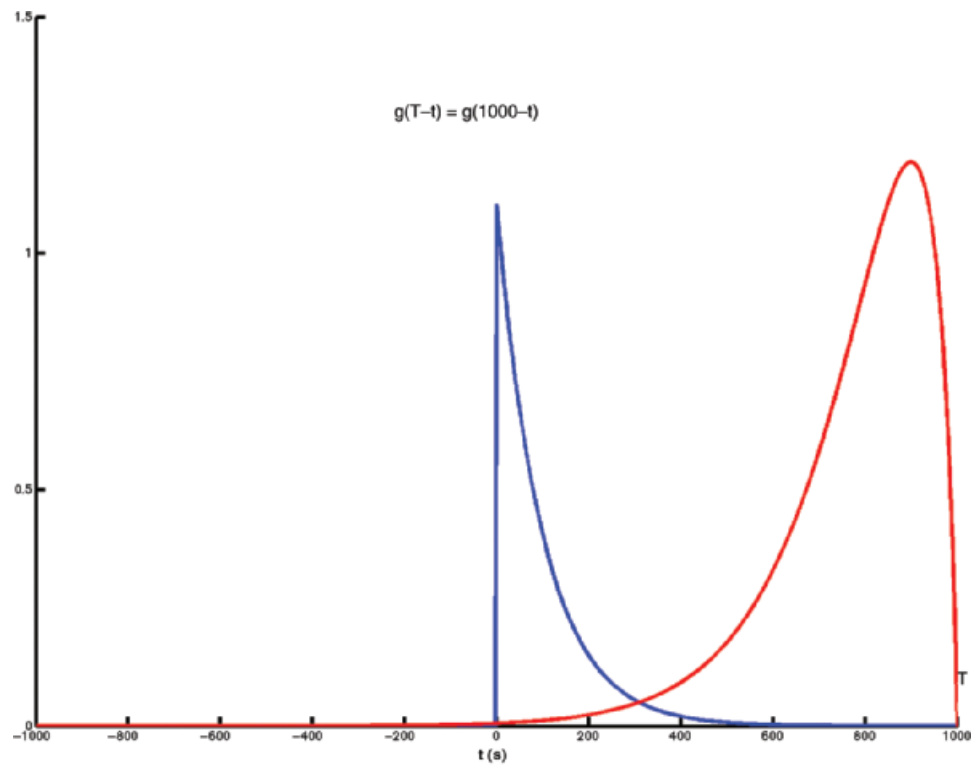
D

Figure 8-2. (Continued) **C-F:** The function $g(T-t)$ is created; T determines the exact position of this function.

6 Perfusion Imaging in Clinical Practice



E



F

Figure 8-2. (Continued)

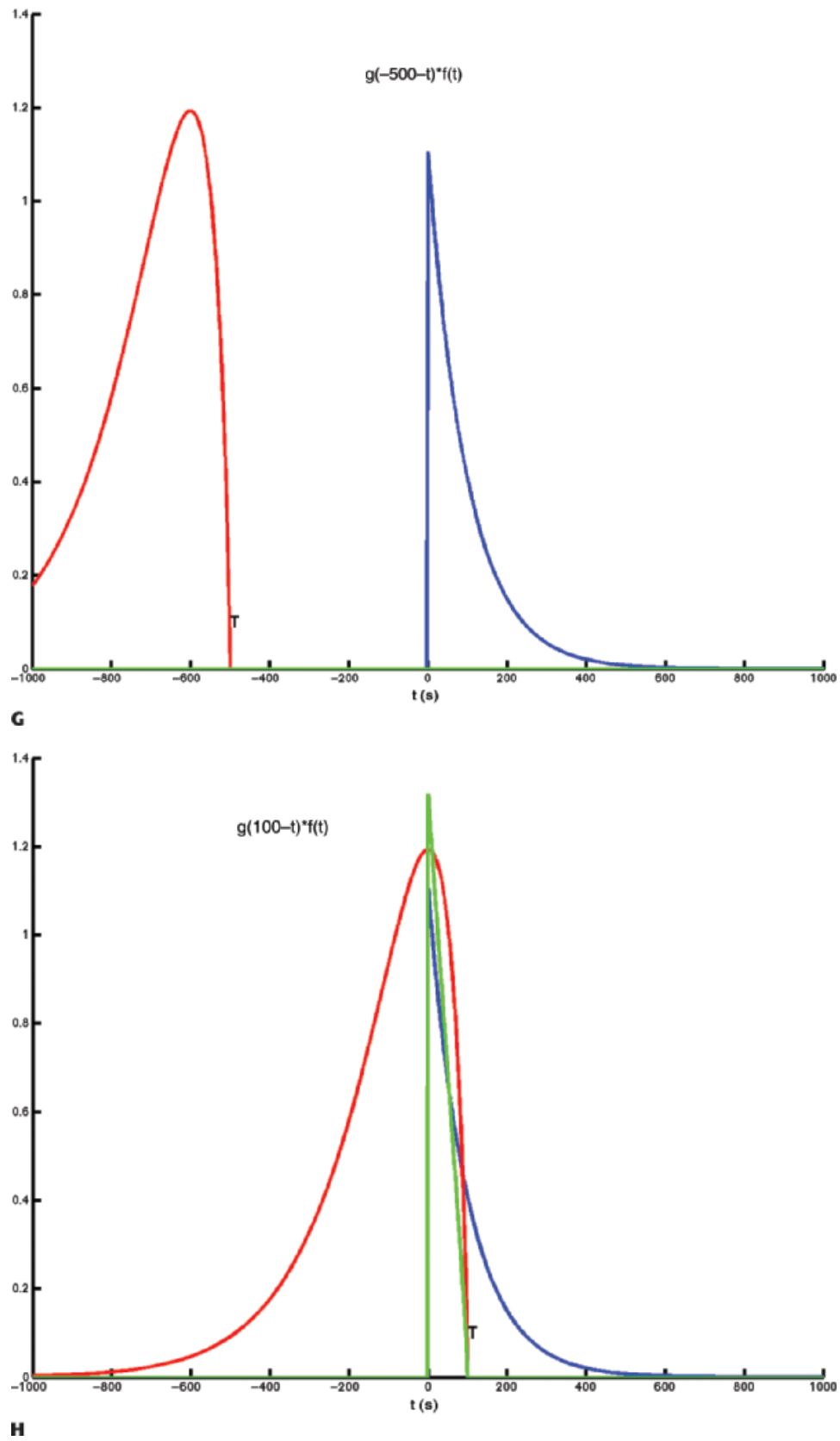


Figure 8-2. (Continued) **G–I:** For any given value of T , the function $g(T - t)$ is multiplied with $f(t)$ for all values of t , giving the green curve.

8 Perfusion Imaging in Clinical Practice

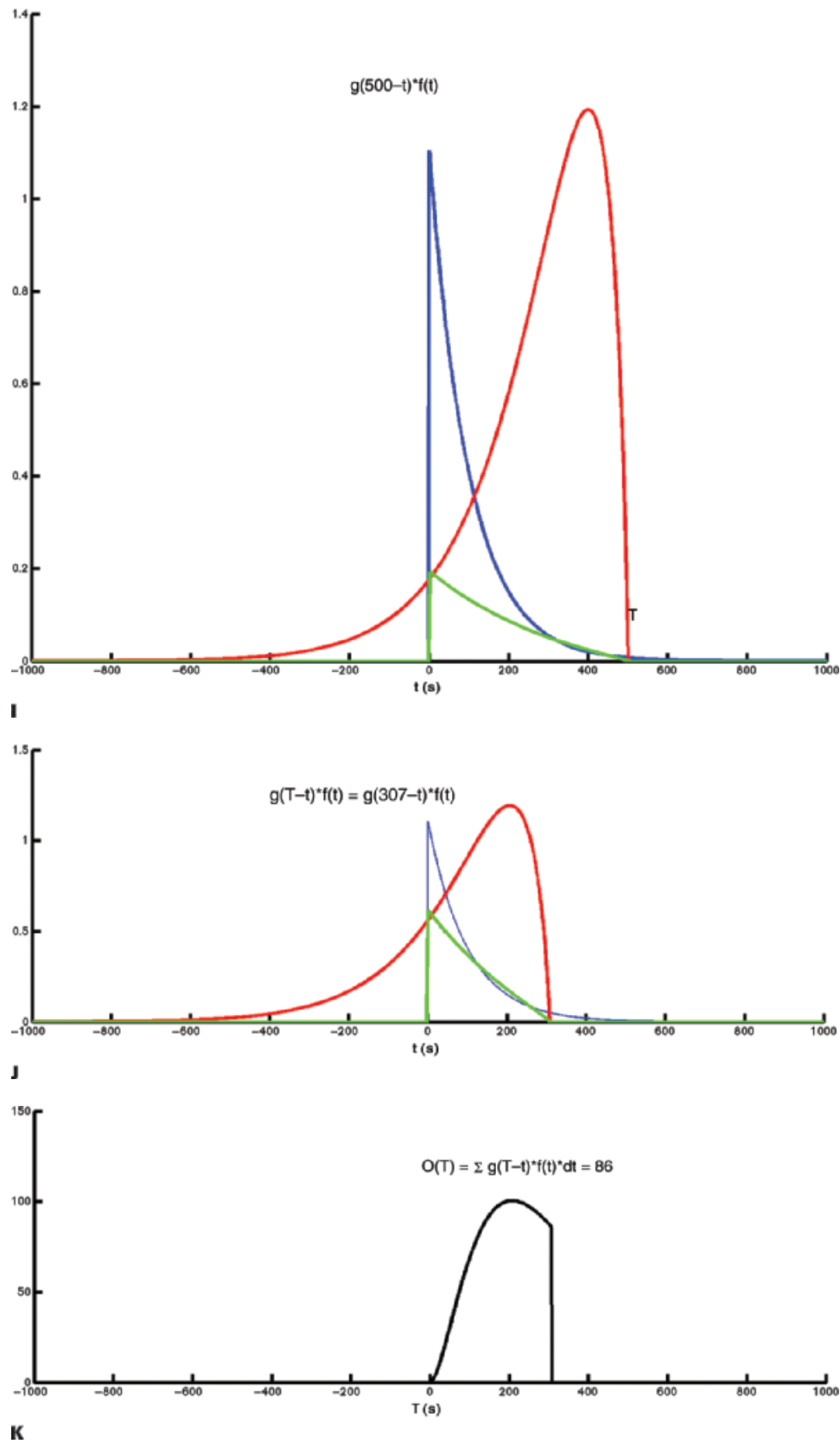


Figure 8-2. (Continued) **J and K:** For a given value of T , the result of the convolution at time T , $O(T)$, is the area under the green curve. At $T = 307$, $O(307) = 86$, which is the area under the green curve. By letting T go through all relevant values, $O(T)$ is calculated for all values of T in that interval. In the figure, $O(T)$ has been calculated up to $T = 307$.

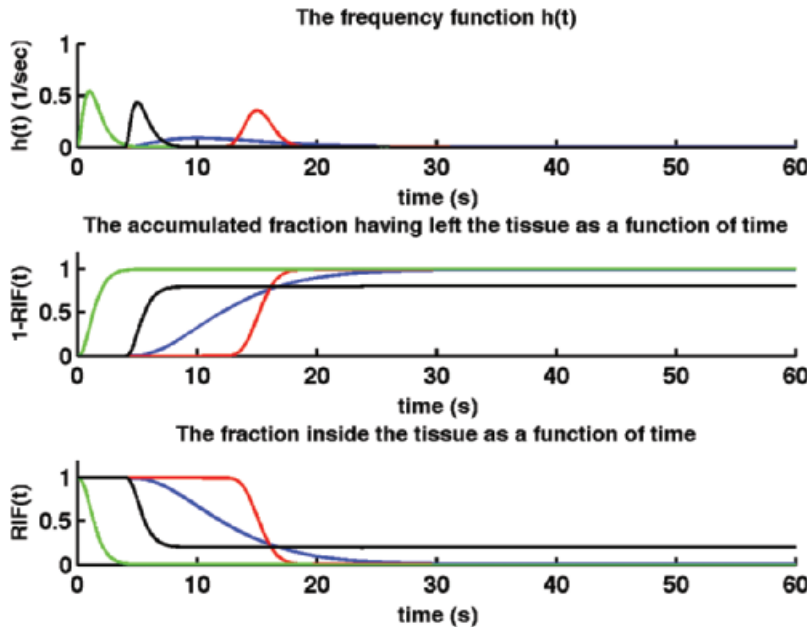


Figure 8-3. Examples of frequency functions, $h(t)$, all modeled as a gamma-variate function, and all but one normalized so area is 1. The black gamma-variate function has an area of 0.8; that is, 20% of the CA is irreversibly trapped in the tissue. Integration of $h(t)$ gives the accumulated fraction, which has left the tissue as a function of time, $1 - \text{RIF}(t)$, while $\text{RIF}(t)$ is the fraction remaining in the tissue as a function of time: The residue impulse response function. Note that $1 - \text{RIF}(t) + \text{RIF}(t) = 1$ for all values of t , and the turning point (the point at which the first derivative change sign) of $\text{RIF}(t)$ and $1 - \text{RIF}(t)$ occurs corresponding to the maximum of the frequency function: $\frac{\partial h(t)}{\partial t} = \frac{\partial^2 \text{RIF}(t)}{\partial t^2} = 0$.

Is the frequency function $h(t)$ clinically interesting? In 1992, Kuschinsky and Paulson suggested that capillary perfusion heterogeneity had a significant impact on capillary diffusion capacity and that the capacity might be increased by homogenization of the perfusion pattern, a response elicited by neurovascular stimulation.¹² This has lately been theoretically substantiated in relation to brain oxygen extraction.¹³ The variance of the frequency function, $h(t)$, is a measure of this kind of capillary heterogeneity.

The partition coefficient λ was mentioned above, and if we use the arterial full blood concentration as a reference concentration, the partition coefficient becomes $\lambda = C_i/C_a$. We could also choose the capillary concentration in the middle of the capillary or the concentration at the outlet (in a vein): $\lambda = C_i/C_v$. Ideally, the definition rests on an equilibrium experiment, but often one assumes instantaneous equilibration so $\lambda = C_i(t)/C_a(t)$. Using the relation

$$\lambda = \frac{\int_0^{\infty} C_i(t) dt}{\int_0^{\infty} C_a(t) dt} \quad (7)$$

the requirement of instantaneous equilibration can be relaxed. In the situation where the CA is confined to the vascular space, that is, no leakage, λ represents the blood volume, for example, in the brain, so λ becomes the cerebral blood volume, CBV. If the CA leaks easily through the capillary membrane, but does not enter the cells, then λ becomes the $v_c + v_b$. Finally, there exists an important relationship between MTT, λ , and f , called the central volume principle: $\text{MTT} = \lambda/f$.¹¹ It can be obtained from our basic tracer kinetic equation using the Laplace transformation

$$L(C_i(t)) = L(C_a(t) \otimes f \text{RIF}(t)) = f L(C_a(t)) L(\text{RIF}(t))$$

using the fact that Laplace transformation of a convolution integral equals the product of the Laplace transformed functions itself, and we also get from Eq. (7)

$$\lambda \frac{L(C_a(t))}{s} = \frac{L(C_i(t))}{s}$$

which inserted in the former equation gives

$$\lambda \frac{L(C_a(t))}{s} = f \frac{L(C_a(t)) L(\text{RIF}(t))}{s} \Leftrightarrow \frac{\lambda}{s} = f \frac{L(\text{RIF}(t))}{s}$$

where we have eliminated $L(C_a(t))$ on each side of the equation. Taking the inverse Laplace transformation on each side of the last equation gives

$$\lambda = f \int_0^{\infty} \text{RIF}(t) dt = f \text{MTT} \Leftrightarrow f = \frac{\lambda}{\text{MTT}} \quad (8)$$

Thus, the central volume principle is correct for any shape of RIF. Above, we have alluded to the information embedded in the RIF. The question is how we can estimate RIF and f . Clearly, we need to sample many concurrent time points of C_a and C_i in order to estimate RIF and f . But we also need a model of the RIF(t), expressed as an analytical mathematical expression, containing our physiologic “free” parameters and which can be found in an optimization procedure.

■ Estimation of RIF by Models

Building a model based on assumptions of the destiny of the CA in the tissue is intimately related to deriving an analytical expression for the RIF, as shown in the following.

Imagine that we have some evidence that all tracer molecules entering as a bolus (ideally as a delta function) and traveling with the same speed (plug flow) through the tissue will leave the tissue (voxel) exactly at the same time T_c . Then, we would build a simple model of RIF as $\text{RIF}(t) = 1$ for $0 < t < T_c$ and $\text{RIF}(t) = 0$ for $t > T_c$. The RIF is shown in Figure 8.4A. If we inject a short bolus with concentration $C_a(0)$ at time zero over a very short time interval Δt , then the tracer kinetic equation will look like

$$\begin{aligned} C_i(t) &= C_a(t) \otimes f \text{RIF}(t) = f C_a(0) \Delta t \quad 0 < t < T_c \\ C_i(t) &= 0 \quad t > T_c \end{aligned}$$

A unit step function, $U(t)$, is defined as

$$\begin{aligned} U(t) &= 1; \quad t \geq 0 \\ U(t) &= 0; \quad t < 0 \end{aligned}$$

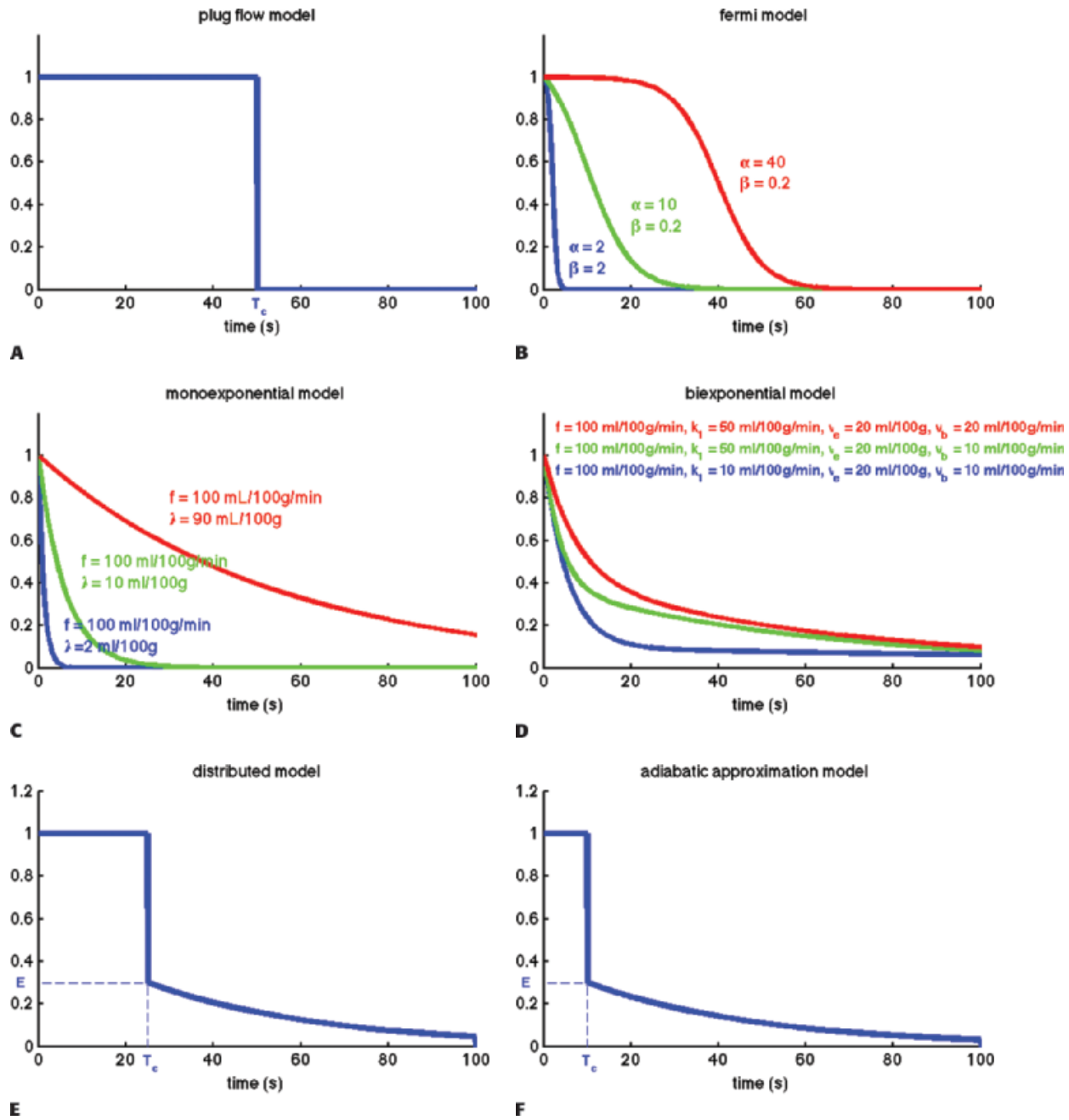


Figure 8-4. Examples of different models of the residue impulse response function. **A:** A simple model based on the assumption that all CA molecules leave the tissue simultaneously. **B:** A Fermi function, the curve is shown for three different sets of values; note the flexibility of the configuration. **C:** A monoexponential model compatible with a one-compartment model; note how the distribution volume, λ , influences the timing of the curve. **D:** A biexponential model compatible with a two-compartment model. Note how k_1 influences the slow component. **E and F:** These models take into account that a CA concentration can be a function of both time and position in a capillary. Essentially, the functions consist of a vascular phase, where a fraction of the CA moves through the tissue like a plug flow and leave the tissue simultaneously, while another fraction leaks into the extravascular space and gradually leaves the tissue afterwards.

Then, the RIF(t) can conveniently be rewritten as

$$\text{RIF}(t) = U(t) - U(t - T_c)$$

A more reasonable assumption is that we have a distribution of transit times where some tracer molecules are somewhat faster than others. The Fermi function may capture this situation, with the expression

$$\text{RIF}(t) = \frac{1 + e^{-\alpha\beta}}{1 + e^{-(t-\alpha)\beta}} \quad (9)$$

having two adjustable parameters, where α determines the plateau (the minimal transit time) and β is related to the decay due to CA leaving the tissue. Note that if $t = 0$, RIF(0) = 1, and after the plateau, the function decays monotonously. The RIF(t) function is shown in Figure 8.4B.

A common approach is to consider the tissue as consisting of one or more compartments. Ideally, a compartment constitutes a volume fraction of the total tissue, where uniform concentration is established so fast at each time point so the concentration can be characterized as $C(t)$, that is, the compartment is well mixed, and a possible slow diffusion within a compartment is ignored. The starting point for compartment analysis is based on an extension of the Fick principle

$$\frac{dQ}{dt} = \sum_m J_{in}^m - \sum_n J_o^n \quad (10)$$

which states that the change in the amount of a CA in a given compartment is equal to the sum of all fluxes in and out of the compartment, where fluxes entering the compartment are positive and fluxes leaving the compartment are negative. As an example, we will derive the transport equation for a freely diffusible tracer. If membranes do not restrict diffusion through the tissue, the tissue (or voxel) will behave, as a one-compartment system, and the change of the amount in the tissue is according to the Fick principle¹⁴

$$\frac{dQ}{dt} = J_{in} - J_o \quad (11)$$

assuming either one inlet and one outlet, or if multiple inlets exist, it will sum up to J_{in} and similar for the outlet. If blood is the source of delivery of the CA, and CA is not produced or metabolized inside the tissue and also leaves by blood plasma, then we have

$$\frac{dQ(t)}{dt} = V_t \frac{dC_t(t)}{dt} = J_{in}(t) - J_o(t) = FC_a(t) - FC_o(t)$$

where V_t is the volume (or the mass) of the tissue, F is the total blood flow entering the tissue in focus (e.g., mL/min), and $C_a(t)$ is the arterial concentration and $C_o(t)$ is the concentration at the outlet. For a freely diffusible CA, it is a reasonable assumption that a fast equilibrium exists between tissue concentration and concentration at the outlet at any time point, giving $\lambda = C_o(t)/C_t(t)$, that is, the partition coefficient. Depending on the particular CA used, λ can be larger, equal, or smaller than V_t . Inserting this relationship results in a solvable first-order differential equation:

$$\frac{dC_t(t)}{dt} = \frac{F}{V_t} C_a(t) - \frac{F}{V_t} \frac{C_t(t)}{\lambda} = fC_a(t) - \frac{f}{\lambda} C_t(t)$$

With the initial conditions that $C_t(0) = 0$, the solutions is

$$C_t(t) = fC_a(t) \otimes \exp\left(-\frac{f}{\lambda}t\right) = f \int_0^t C_a(\tau) \exp\left(-\frac{f}{\lambda}(t-\tau)\right) d\tau \quad (12)$$

This equation is appropriate for labeled water or radioactive xenon. Thus, the RIF is a simple monoexponential function (see Fig. 8.4C) with two physiologic constants, the perfusion and the partition coefficient. If the time course of the tissue concentration and the arterial concentration as a function of time are measured, then these two constants can easily be estimated using standard fitting procedures. This equation is based on the pioneering work of Kety.¹⁰

In the MR field, we are not so lucky as to have a freely diffusible CA yet. In, for example, muscle tissue, the extraction fraction during the first pass is around 50% to 60%; in the liver, it is probably higher; and in the brain, it is close to zero. For an MR CA, which is confined to the plasma volume, the equation will be

$$\frac{dQ(t)}{dt} = V_t \frac{dC_t(t)}{dt} = J_{in}(t) - J_o(t) = F^p C_a^p(t) - F^p C_o^p(t)$$

where F^p is the blood plasma flow entering the tissue in focus (e.g., mL/min), $C_a^p(t)$ is the arterial plasma concentration, and $C_o^p(t)$ is the plasma concentration at the outlet. The conversion to full blood is given by

$$F^p = (1 - \text{Hct}_{sv})F, \quad C_a^p(t) = \frac{C_a(t)}{1 - \text{Hct}_{lv}} \quad (13)$$

where Hct_{sv} and Hct_{lv} are the small-vessel hematocrit and large-vessel hematocrit, respectively. The small-vessel hematocrit is used in conjunction with F because F relates to the microcirculation within the tissue, while the large-vessel hematocrit in conjunction with the input function relates to measurements in larger arteries. If we still can assume that $\lambda = C_o(t)/C_o^p(t)$, we end up with a similar equation as Eq. (12):

$$\frac{dC_t(t)}{dt} = \frac{F^p}{V_t} C_a^p(t) - \frac{F^p}{V_t} \frac{C_t(t)}{\lambda} = f^p C_a^p(t) - \frac{f^p}{\lambda} C_t(t)$$

With the initial condition that $C_t(0) = 0$, the standard solution is

$$\begin{aligned} C_t(t) &= f^p \int_0^t C_a^p(\tau) \exp\left(-\frac{f^p}{\lambda}(t-\lambda)\right) d\tau = \\ &= f^p C_a^p(t) \otimes \exp\left(-\frac{f^p}{\lambda}t\right) = \\ &= \frac{(1 - \text{Hct}_{sv})}{(1 - \text{Hct}_{lv})} f C_a(t) \otimes \exp\left(-\frac{(1 - \text{Hct}_{sv})f}{\lambda}t\right) \end{aligned} \quad (14)$$

In fact, Eq. (14) has been used for brain perfusion with assumed intact BBB, and here, the MR CA behaves as an intravascular CA. Then, the partition coefficient λ is a measure of the cerebral blood volume, CBV. An example is shown in Figure 8.5. Whether one can use an intravascular CA for measurement of brain perfusion is controversial, because the results obtained are restricted by the assumption of the monoexponential RIF and may bias the results as pointed out by Lassen¹⁵ and Weisskoff et al.,¹⁶ and it is also uncertain which part of the vascular system is actually being measured. At least, it would be preferable to be able to model the RIF with a higher degree of freedom or without specifying an analytic model at all (see later).

In many types of tissues, the extraction fraction is neither very low nor very high. In, for example, the heart muscle tissue, the extraction fraction during the first pass is around 50% to 60%, and the models above might not be the most appropriate in this situation. A two-compartment model is a better description of the transport of the CA. Here, we let these two compartments be represented by the blood plasma in tissue, V_p , with the CA plasma concentration $C_p(t)$ in the tissue and the extravascular extracellular space in the tissue with volume V_e , with a CA concentration $C_e(t)$ (see Fig. 8.6). Note the assumption of the blood volume being represented by just one concentration regardless of the location along the capillary. Using the Fick principle and assuming first-order diffusion between compartments, the transport equations for the two compartments are

$$\begin{aligned} V_p \frac{dC_p(t)}{dt} + (F + K_1)C_p - K_1 C_e &= FC_a(t), \\ V_e \frac{dC_e(t)}{dt} - K_1 C_p + K_1 C_e &= 0 \end{aligned} \quad (15)$$

Here, F and K_1 denote *plasma* perfusion and *plasma* clearance, respectively, and $C_a(t)$ is arterial plasma concentration (we omit the superscript for graphical reasons). In addition, we have the following relationships:

$$\begin{aligned} V_e C_e &= V_{tis} C_{tis} \\ V_p C_p &= (V_p + V_{Hct}) C_b \Leftrightarrow C_b = (1 - \text{Hct}_{sv}) C_p \\ V_t &= V_{tis} + V_p + V_{Hct} \\ 1 &= v_{tis} + v_p + v_{Hct} \\ C_t &= \frac{Q}{V_t} \end{aligned}$$

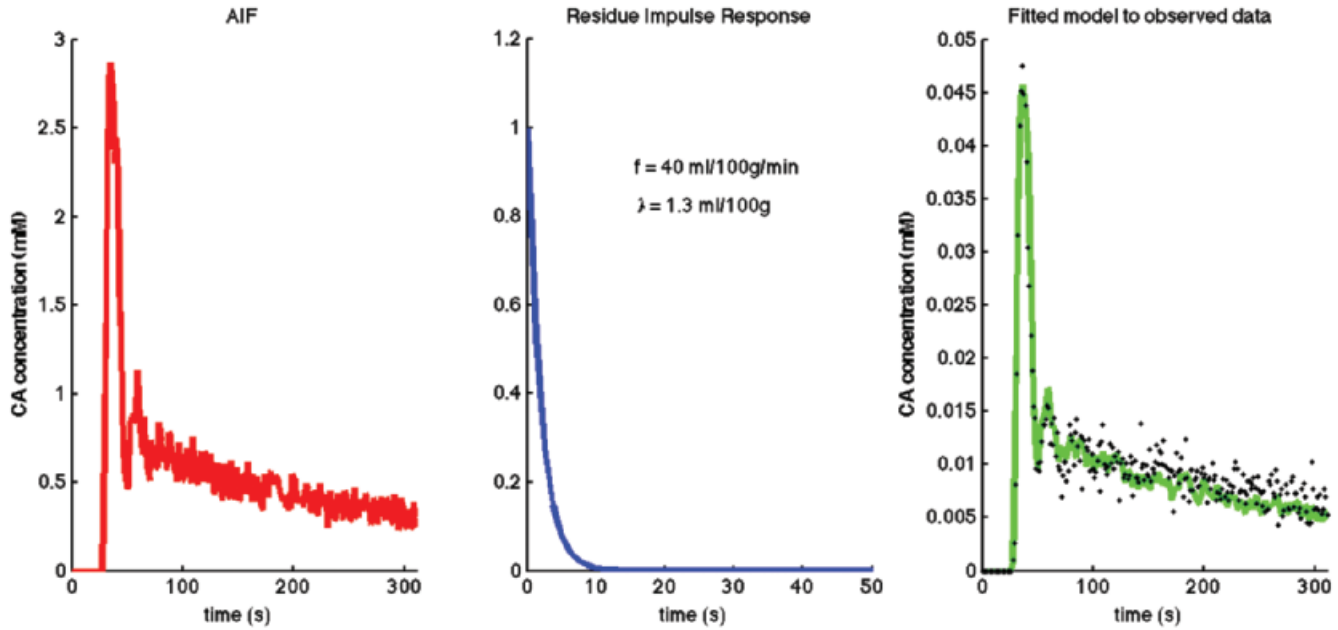


Figure 8-5. The arterial input function, AIF, is obtained from the internal carotid artery. Observed data are the tissue concentration enhancement obtained from an ROI placed in brain cortical gray matter. The green curve is a one-compartment model fitted to the data, that is, the AIF convolved with the residue impulse function of a one-compartment system. Optimum of the two free parameters, f and λ , is shown. Because the CA is nearly confined to the vascular space because of the blood–brain barrier, λ , is a measure of the cerebral blood volume in the ROI.

stating that the total tissue volume is composed of the extravascular tissue with volume, V_{tis} , the plasma volume, V_p , and the cell blood volume, V_{Hct} . It is assumed that the MR CA diffuses fast in the extravascular interstitial space. The second differential equation of Eq. (15) can be solved as done previously and gives

$$C_e(t) = \frac{K_1}{V_e} C_p(t) \otimes \exp\left(-\frac{K_1}{V_e} t\right)$$

which inserted in the first differential equation gives

$$V_p \frac{dC_p(t)}{dt} + (F + K_1) C_p - \frac{K_1}{V_e} C_p(t) \otimes \exp\left(-\frac{K_1}{V_e} t\right) = FC_a(t)$$

If we apply the Laplace transformation, then we can isolate $L(C_p(t))$ and $L(C_e(t))$, which we are searching for

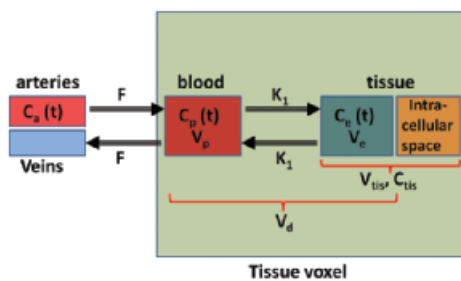


Figure 8-6. A two-compartment model. Such a model may be relevant for a moderate degree of leakiness. If k_1 is zero or very high, a one-compartment model might be more useful. Using a two-compartment model in this situation may result in so-called overfitting and less reliable results.

$$L(C_p) \left(sV_p + (F + K_1) - \frac{K_1}{sV_e + K_1} \right) = FL(C_a) \Leftrightarrow L(C_p) = \frac{s/V_p + K_1/V_p V_e}{s^2 + s(K_1/V_e + F/V_p + K_1/V_p) + FK_1/V_e V_p} FL(C_a)$$

$$L(C_e) = \frac{K_1}{sV_e + K_1} L(C_p) = \frac{K_1}{V_e V_p s^2 + s(K_1/V_e + F/V_p + K_1/V_p) + FK_1/V_e V_p} FL(C_a)$$

Using the Laplace transformation of exponentials as

$$L(A \exp(-at) + B \exp(-bt)) = \frac{A}{s+a} + \frac{B}{s+b}$$

$$L\left(\frac{\exp(-bt) - \exp(-at)}{a-b}\right) = \frac{1}{(s+a)(s+b)}$$

we can identify

$$A = \frac{V_e \alpha - K_1}{V_e V_p (\alpha - \beta)}; \quad B = -\frac{V_e \beta - K_1}{V_e V_p (\alpha - \beta)}$$

$$\alpha = \frac{1}{2} \left(\frac{K_1}{V_e} + \frac{F + K_1}{V_p} + \sqrt{\left(\frac{K_1}{V_e} + \frac{F + K_1}{V_p} \right)^2 - 4 \frac{FK_1}{V_e V_p}} \right)$$

$$\beta = \frac{1}{2} \left(\frac{K_1}{V_e} + \frac{F + K_1}{V_p} - \sqrt{\left(\frac{K_1}{V_e} + \frac{F + K_1}{V_p} \right)^2 - 4 \frac{FK_1}{V_e V_p}} \right)$$

and $C_p(t)$ and $C_e(t)$ are then

$$C_p(t) = FC_a(t) \otimes \frac{1}{V_e V_p (\alpha - \beta)} \left((V_e \alpha - K_1) \exp(-\alpha t) - (V_e \beta - K_1) \exp(-\beta t) \right)$$

$$C_e(t) = FC_a(t) \otimes \frac{1}{V_e V_p (\alpha - \beta)} \left(K_1 \exp(-\beta t) - K_1 \exp(-\alpha t) \right)$$

Total tissue concentration, $C_t(t)$, is then found from

$$V_t C_t(t) = V_p C_p(t) + V_e C_e(t) \Rightarrow C_t(t) = \frac{F}{V_t} C_a(t) \otimes \frac{1}{\alpha - \beta} \left(\left(\alpha - \frac{K_1}{V_e} - \frac{K_1}{V_p} \right) \exp(-\alpha t) + \left(\frac{K_1}{V_e} + \frac{K_1}{V_p} - \beta \right) \exp(-\beta t) \right) \quad (16)$$

where $f = F/V_t$, and conveniently, all other constants are normalized by V_t . Conversion to full blood reference is also straightforward. Note that the residue impulse response function is biexponential and $RIF(0) = 1$ (see Fig. 8.4D). The two-compartment model has four free parameters: f^p , k_1^p , v_e , and v_p . This type of model has previously been applied to a number of diseases in different organs including the brain lately.^{8,17} Brix already presented a simplified version of the two-compartment model in 1991.¹⁸ An example of using this model in a leaky brain tumor is shown in Figure 8.7.

The first tracer kinetic model, often called the Tofts model, used in conjunction with MRI, focused on estimation of BBB permeability of multiple sclerosis plaques and brain tumors^{19,20}:

$$C_t(t) = k_1^p C_a^p(t) \otimes \exp\left(-\frac{k_1^p}{\lambda} t\right) = K^{\text{trans}} \frac{C_a(t)}{(1 - \text{Hct}_{LV})} \otimes \exp\left(-\frac{K^{\text{trans}}}{v_e} t\right) \quad (17)$$

Note that $K^{\text{trans}} (= k_1^p = Ef^p)$ is the tissue clearance (tissue uptake transfer constant) with reference to plasma with the dimension mL plasma cleared/100 mL tissue/min (a capital letter in K^{trans} is traditional used), $C_a^p(t)$ is plasma concentration of the CA, while $C_a(t)$

is full blood concentration. The assumptions behind this model are, firstly, that the vascular volume fraction in the tissue is vanishing small and can be ignored and, secondly, that the arterial plasma concentration of the CA represents the input function to a distribution volume, which is equivalent with the extravascular extracellular space, v_e . Note that if $ps \gg f$ ($E = 1$), then $K^{\text{trans}} = f^p$, and we are back to Eq. (12). If $ps \ll f$ ($E \rightarrow 0$), $K^{\text{trans}} = ps$. Thus, the residue impulse response function in this case is $RIF(t) = \exp(-K^{\text{trans}} t/v_e)$. After the introduction of Eq. (17), it was quickly being used outside the brain, and it soon became clear that the vascular component could not be ignored and constituted a significant part of the MR signal in many types of tissue, for example, in the heart.²¹ In order to ameliorate this situation, the vascular volume was included giving the following equation, often denoted as the extended Tofts model²²:

$$C_t(t) = v_p C_a^p(t) + k_1^p C_a^p(t) \otimes \exp\left(-\frac{k_1^p}{v_e} t\right) \quad (18)$$

The specific assumption associated with this expression is that the plasma fraction in the tissue has a CA concentration equal with the arterial plasma concentration (which is measured), and the loss from the vascular space due to leakage is so small that it can be ignored; obviously, this equation implicitly suggests a very small $k_1^p \approx ps$ product. The extended Tofts model has three unknown free parameters: k_1^p , v_e , and v_p . Formally, the $RIF(t) = v_p \delta(t) + \exp(-K^{\text{trans}} t/v_e)$.

It is increasingly being recognized that Eq. (18) in some situation is inadequate to describe the CA transport in some type of tissues, or at least, the interpretation of k_1^p is somewhat ambiguous, as it is often correlated with both perfusion and permeability.^{23–25} It has even been shown that a good fit of Eq. (18) to data is no guaranty of obtaining accurate results,²⁴ and more elaborate methods should probably be used (see below).

Equation (18) is a good starting point for deriving the famous Patlak equation.²⁶ If leakage is unidirectional, that is, negligible backflux, then $RIF(t) = 1$, and Eq. (18) becomes

$$C_t(t) = v_p C_a^p(t) + k_1^p \int_0^t C_a^p(\tau) d\tau$$

Again, the assumptions are a unidirectional transport, that is, an irreversible leakage, and the arterial plasma with concentration

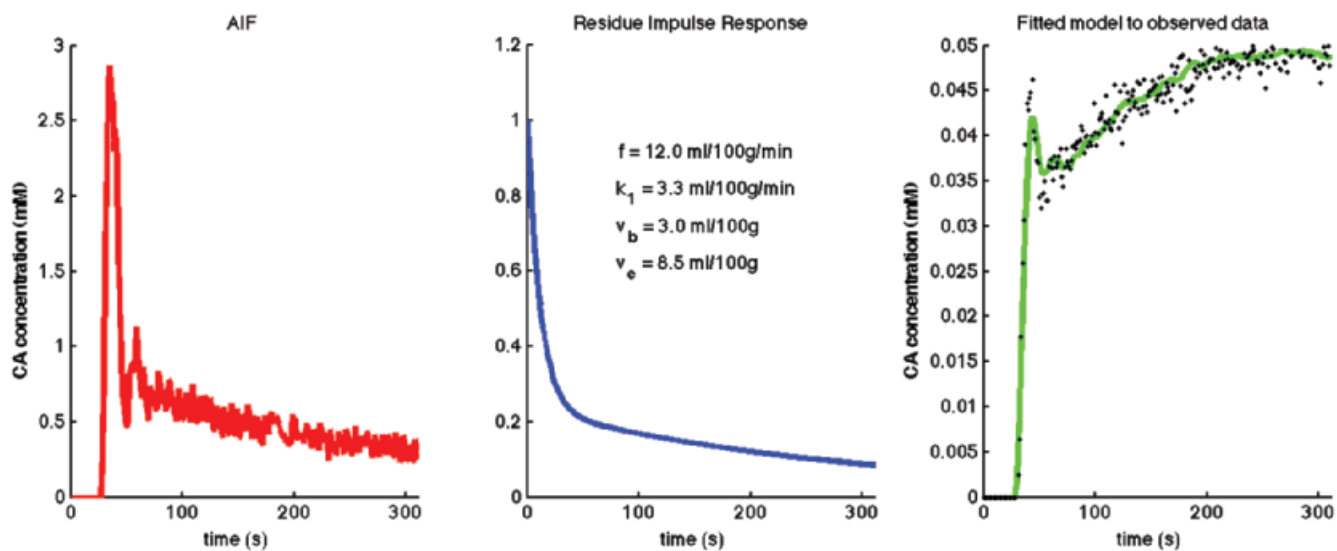


Figure 8-7. Observed data are the tissue concentration enhancement obtained from an ROI placed in a brain tumor. Note that data show a pronounced “vascular” peak followed by a steadier enhancement due to deficiency of the BBB. The green curve is two-compartment model fitted to the data, that is, the AIF convolved with the residue impulse function of a two-compartment system. Optimum of the four free parameters is shown.

14 Perfusion Imaging in Clinical Practice

$C_a^p(t)$ serves as a source for the leakage inside the tissue, and importantly, the CA loss from this vascular space is so small that it can be ignored. Obviously, for an inert typical MR CA agent, $k_1^p = ps$ product. Dividing both sides of the equation with the instantaneous $C_a^p(t)$ results in the Patlak equation

$$\frac{C_t(t)}{C_a^p(t)} = v_p + k_1^p \frac{\int_0^t C_a^p(\tau) d\tau}{C_a^p(t)} \quad (19)$$

If one then plots the ratio $C_t(t)/C_a^p(t)$ as a function of $\int_0^t C_a^p(\tau) d\tau / C_a^p(t)$, one will get a straight line with the slope k_1^p and an intercept of v_p , which are the two unknown in this equation. As pointed out by Patlak, v_p in reality includes the steady-state volume of distribution of all reversible compartments. The Patlak analysis has been used successfully in many nuclear medicine studies and seems also useful when measuring the BBB permeability in the brain when using DCE-MRI.^{17,27} However, it is important to restrict its use in accordance with the assumptions. When used, one will notice an initial phase in the Patlak plot, which is related to a vascular transition, and the Patlak equation only relates to the slowly steady increase afterwards (see Fig. 8.8). In order to understand the entire curve obtained, it is more instructive to start with the two-compartment model, eliminating all terms related to the back-diffusion, which we now assume can be neglected:

$$V_p \frac{dC_p(t)}{dt} + (F + K_1)C_p = FC_a(t),$$

$$V_e \frac{dC_e(t)}{dt} - K_1 C_p = 0$$

$$V_t C_t(t) = V_e C_e(t) + V_p C_p(t)$$

Solving these coupled differential equations using the Laplace transformation as previously, and where F, K_1 , and C_a relate to plasma, gives

$$\begin{aligned} C_p(t) &= \frac{F}{V_p} C_a(t) \otimes \exp\left(-\frac{F+K_1}{V_p} t\right) \\ C_e(t) &= \frac{FK_1}{V_e(F+K_1)} C_a(t) \otimes \left(1 - \exp\left(-\frac{F+K_1}{V_p} t\right)\right) \\ C_t(t) &= \frac{F}{V_t} C_a(t) \otimes \left[\frac{K_1}{F+K_1} + \frac{F}{F+K_1} \exp\left(-\frac{F+K_1}{V_p} t\right)\right] \end{aligned} \quad (20)$$

$f^p = F^p/V_t$ and all other constants can be normalized to V_t . Note that the RIF(0) = 1. Furthermore, if $F^p \gg K_1^p$, as will be the case for a unidirectional transport of an inert MR CA, then we get

$$C_t(t) \approx k_1^p \int_0^t C_a^p(\tau) d\tau + f^p \int_0^t C_a^p(\tau) \exp\left(-\frac{f^p + k_1^p}{v_p} (t - \tau)\right) d\tau \quad (21)$$

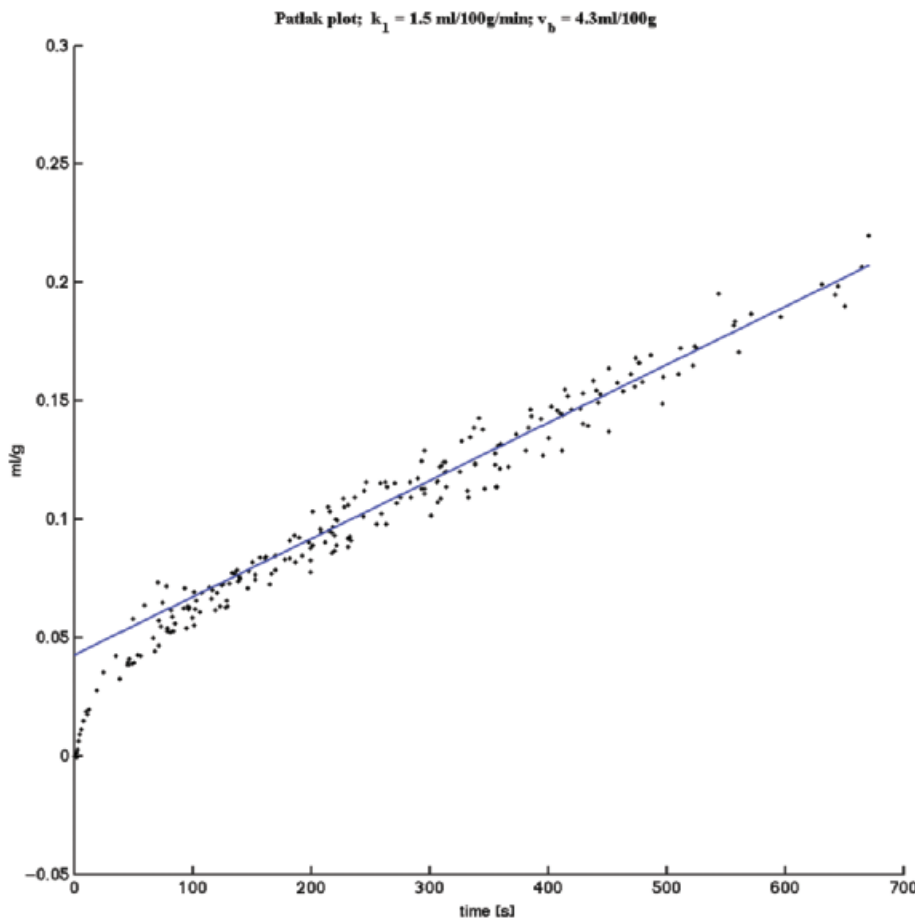


Figure 8-8. An example of a Patlak plot:

$\frac{C_t(t)}{C_a^p(t)}$ as a function of $\frac{\int_0^t C_a^p(\tau) d\tau}{C_a^p(t)}$. The

slope of the regression line corresponds to k_1 , while the intercept corresponds to the blood plasma volume v_p . Data obtained from a leaky brain tumor.

Obviously, k_1^p is the ps^p product. It is seen that the initial part in a Patlak plot is related a vascular phase, which eventually vanished leaving a term $k_1^p \int C_a^p(\tau) d\tau$, which is related to a steady irreversible accumulation of the CA in the extravascular extracellular tissue. Equation (20) can in fact be used as a model and fitted to data, when back-diffusion can be ignored. The model has three free parameters: f^p , ps^p , and v_p ; however, v_e cannot be estimated. Finally, it is important to inspect the Patlak plot: If the straight line, corresponding to the steady increase, tends to level off for later time points, then this is an indication of a possible back-diffusion. In fact, if the uptake is followed for very long time, back-diffusion will eventually occur. In that perspective, fitting of Eq. (16) to such data seems more appropriate.

The assumption of a uniform well-mixed vascular concentration is an approximation and can potentially introduce a bias. In reality, one can imagine that the capillary concentration changes as a function of position along the capillary in addition to being a function of time.^{28,29} Incorporation of time and position constitutes the so-called distributed model, signifying that concentration gradients exist within the tissue, which is in contrast to compartment models where every compartment is well mixed instantaneously and concentration is only a function of time. The starting point for this model is related to the concentration inside the capillary at location x with a total length L :

$$V_p \frac{\partial C_p(t,x)}{\partial t} = -FL \frac{\partial C_p(t,x)}{\partial x} - PS(C_p(t,x) - C_e(t,x)) + FLC_a(t)\delta(x)$$

where we have used the same consideration as when deriving the Crone-Renkin equation. The equation for the extravascular extracellular space is given as

$$V_e \frac{\partial C_e(t,x)}{\partial t} = PS(C_p(t,x) - C_e(t,x))$$

The model assumes plug flow, meaning that every cross section at location x of the capillary have the same uniform concentration characterized by $C_p(t,x)$ and in addition no significant extravascular diffusion along the capillary. The solution to the differential equations using the Laplace transformation results in a residue impulse response function consisting of two parts:

$$\begin{aligned} RIF(t) &= RIF_1(t) + RIF_2(t - T_c) \\ RIF_1(t) &= U(t) - U(t - T_c) \\ RIF_2(t) &= U(t) \left(1 - \exp\left(-\frac{PS}{F}\right) \left(1 + \int_0^t \exp\left(-\frac{PS}{V_e F} \tau\right) \sqrt{\frac{PS^2}{V_e F \tau}} I_1 \sqrt{\frac{PS^2}{V_e F} \tau} d\tau \right) \right) \end{aligned} \quad (22)$$

I_1 is the modified Bessel function. Although the solution is cumbersome, the interpretation is straightforward (see Fig. 8.4E). The first part, $RIF_1(t)$, until T_c corresponds to a fraction of the CA staying inside the vessels and moving forward as a plug flow and leaving the tissue at T_c . This may be called the vascular transit phase. During this phase, another fraction can leave the vascular space into the extravascular space, still contributing to the total amount in tissue. When the vascular phase ends, the RIF is dominated by a slow back-diffusion from the parenchyma corresponding to the leakage fraction, $RIF_2(t)$, signifying loss of CA by perfusion. The transition is a direct measure of E , and the mean transit time of the vascular space and the extravascular space can be found as the area of the respective RIF, which correspond to $MTT = v_p/f^p$ and $MTT = v_e/f^p$, respectively.³⁰ The distributed model has not been thoroughly validated and compared to a two-compartment model, but several studies report a better fit to observed data in brain tumors,³¹ in infarcted myocardium,³² and in neuroendocrine hepatic metastases.³³ It is

likely that the model is highly dependent on the assumption of plug flow, meaning no radial gradient in capillary during the initial wash-in and also a high time resolution, at the level of a second, in order to define the vascular phase with sufficient accuracy. Two variants of the distributed model exist. The first is the so-called tissue homogeneity model, where the extravascular compartment model is treated as a well-mixed compartment and therefore only a function of time.³⁴ However, this does not ease the solution. The second is the so-called adiabatic approximation, where the vascular phase is assumed to be much faster than the leakage process, and leakage occurs only at the venous end of the capillary.³⁵ This leads to a considerable simplification with a residue impulse response function as

$$\begin{aligned} RIF(t) &= 1 \quad 0 \leq t < T_c \\ RIF(t) &= E \exp\left(-\frac{EF}{V_e}(t - T_c)\right) \quad t \geq T_c \end{aligned} \quad (23)$$

It is evident that the initial vascular phase is similar to the original model, but the wash-out phase is substituted by an exponential function (see Fig. 8.4F). The adiabatic approximation model was implemented and validated using D_2O and MRI, and for this setup, perfusion seems to be underestimated for higher value of perfusion.³⁶

In the models presented above, we have assumed a one-capillary model, that is, one typical capillary is representative for all the capillaries in a given voxel or tissue region of interest (ROI). However, multiple-pathway models have been proposed consisting of many capillaries with different flow distribution and length, and each capillary can be characterized by, for example, a distributed model.³⁷ The degree of clinical impact of these elaborated models is up to future research and will probably benefit from an increasing time and spatial resolution of MRI.

■ Estimation of RIF without a Model

So far, it is clear that estimating perfusion or permeability necessitates building a model based on some specific assumptions of how tissue is “handling” the CA used. It is also clear that any model will influence the results obtained using that model. In addition, it is difficult to prove that one model is more accurate compared to another, and even microsphere injection or radioactive water ($^{15}H_2O$) in conjunction with PET, normally considered as a gold standard, has its limitations.³⁸ However, if a model gives useful clinical results, then accuracy might be secondary.

In order to circumvent the problem of specifying a model, model-free or data-driven solution is increasingly being used. The starting point is based on the fact that a convolution can be written in a discrete form as a matrix equation:

$$\bar{y} = f \Delta t \mathbf{A} \bar{x} \quad (24)$$

Here, \bar{y} is a column vector representation of C_t , \mathbf{A} is a matrix representation of C_a , and \bar{x} is a column vector representation of the RIF. Specifying the entries of the matrix equation, it looks like

$$\begin{bmatrix} C_t(1) \\ C_t(2) \\ C_t(3) \\ \vdots \\ C_t(N) \end{bmatrix} = f \Delta t \begin{bmatrix} C_a(1) & 0 & 0 & \dots & 0 \\ C_a(2) & C_a(1) & 0 & \dots & 0 \\ C_a(3) & C_a(2) & C_a(1) & \dots & 0 \\ \vdots & \vdots & \vdots & \ddots & \vdots \\ C_a(N) & C_a(N-1) & C_a(N-2) & \dots & C_a(1) \end{bmatrix} \begin{bmatrix} RIF(1) \\ RIF(2) \\ RIF(3) \\ \vdots \\ RIF(N) \end{bmatrix} \quad (25)$$

Obviously, the equation is discretized with a total of N samples and with a time resolution of Δt . Scrutinizing this equation will disclose the nature of the convolution, however, in a discrete form. For information about matrix calculus, see Glodberg, or for a compact tutorial, see Larsson HBW: Introduction to the general linear model used in fMRI. In fact, Eq. (25) is the typical computer realization of the convolution, where the RIF may be specified by an analytical expression. For example, let $\text{RIF}(i) = \exp(-f \Delta t(i-1)/\lambda)$, $i = 1, \dots, N$; then, this can be used in an optimization procedure, where the model is specified by having a monoexponential residue impulse response function, with two free parameters, f and λ , and with N samples of C_i and C_e . The optimization problem can then be formulated as minimizing the following term:

$$\min \left\{ \left\| \bar{y}^{\text{obs}} - \bar{y}^{\text{calc}} \right\|^2 \right\}$$

where \bar{y}^{obs} is the measured tissue concentration and A represents the measured arterial input function. Then $\bar{y}^{\text{obs}} = \bar{y}^{\text{calc}} + \bar{\epsilon}$, with $\bar{y}^{\text{calc}} = f \Delta t A \bar{x}$, the calculated tissue concentration using the model \bar{x} . The value of f and λ , which minimized the difference between the observed and the calculated tissue concentration, that is, the error or residual $\|\bar{\epsilon}\|$, is said to constitute the optimal solution.

However, Eq. (25) offers another solution. Under some circumstances, it is possible to isolate the $\text{RIF}(i)$ giving a direct solution if the matrix A can be inverted:

$$\bar{y} = f \Delta t A \bar{x} \Rightarrow \bar{x} = \frac{1}{f \Delta t} A^{-1} \bar{y}$$

From matrix algebra, we know that a unique solution is possible if the determinant of the matrix A is different from zero, equivalent

with all the columns of the matrix are linearly independent, that is, the matrix has the rank of N . However, this lucky situation is seldom satisfied due to noise, and perhaps interpolation (see later), and the matrix becomes what is called singular, or rank deficient. Luckily, a solution can always be found in a reduced dimensional space, using the singular value decomposition (SVD) obtaining the pseudo-inverse matrix A^- :

$$\bar{y}^{\text{obs}} = f \Delta t A \bar{x} + \bar{\epsilon} \Rightarrow \bar{x} = \frac{1}{f \Delta t} A^- \bar{y}^{\text{obs}} \Rightarrow \bar{y}^{\text{calc}} = A A^- \bar{y}^{\text{obs}}$$

It can be shown that this solution also minimizes the residuals, that is, the distance between the observed tissue concentration and calculated tissue concentration. Leif Østergaard was the first to introduce this technique in the MR community focusing on perfusion measurements using exogenous CA and tracer kinetic theory.³⁹ For information about SVD, see Glodberg, or for a compact tutorial, see Larsson HBW: Introduction to the general linear model used in fMRI. An example of using the SVD in order to estimate perfusion in the brain is shown in Figure 8.9.

The use of the pseudoinverse comes at a price: the solution is extremely sensitive towards noise, and the unphysiologic oscillation of the RIF is a manifestation of the noise sensitivity. In order to suppress these spurious oscillations, one can select an empirical threshold below which, all eigenvalues are set to zeros, for example, the 20% lowest eigenvalues are set to zeros, at a price of underestimating the perfusion. Thus, the threshold setting is a trade-off between unwanted unphysiologic oscillations and distortions of the RIF and overfitting at one side and a blunted RIF and underestimation of perfusion f at the other side, see Figure 8.9. Another possibility is to directly incorporate our theoretical knowledge about the RIF,

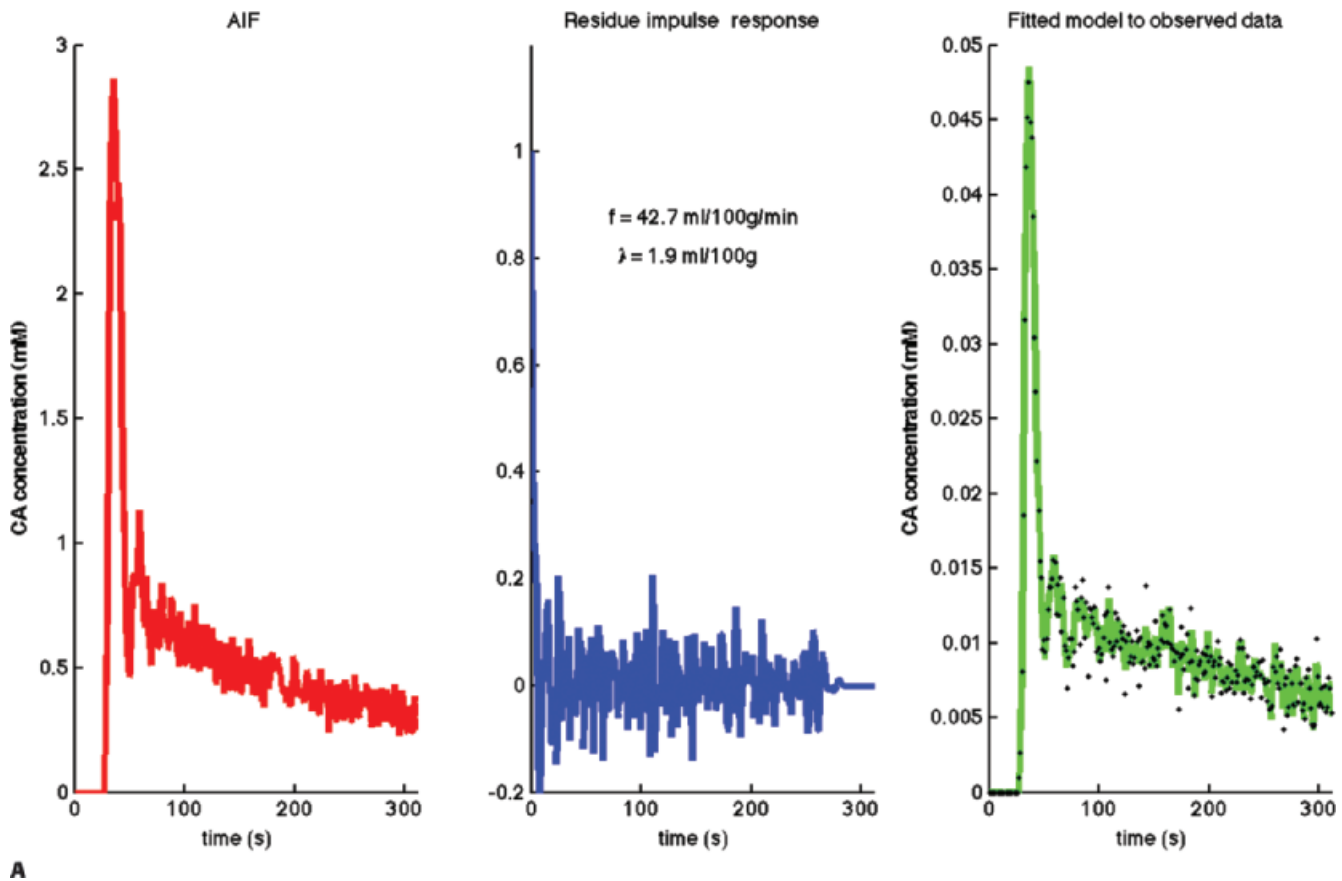


Figure 8-9. Example of the use of the singular value decomposition (SVD). AIF and observed data are the same as in Figure 8.5. **A:** SVD keeping nearly all eigenvalues, that is, no regularization, results in a noisy residue impulse response function and a tendency of overfitting of data.

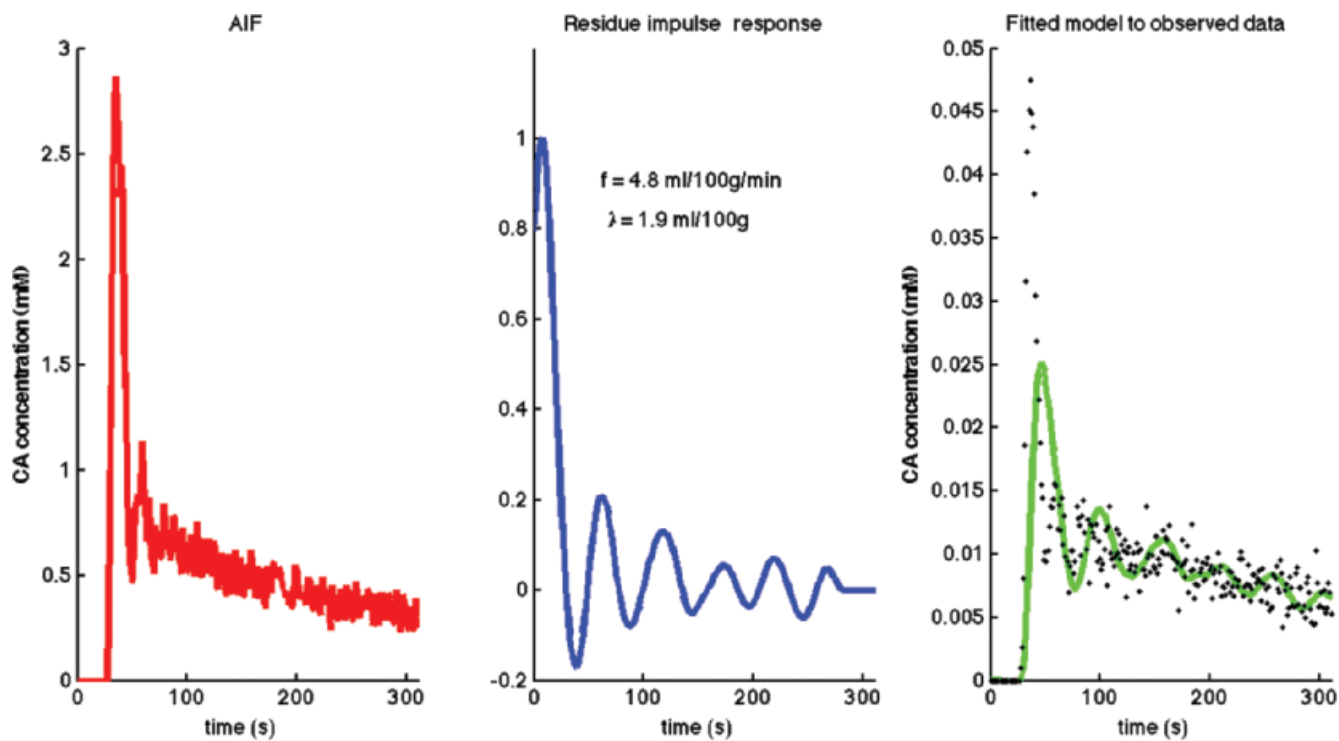


Figure 8-9. (Continued) **B:** Keeping only eigenvalues larger than 20% of the first (largest) eigenvalue results in a less noisy residue impulse response function, however, still having spurious oscillations and a considerable underestimation of brain perfusion.

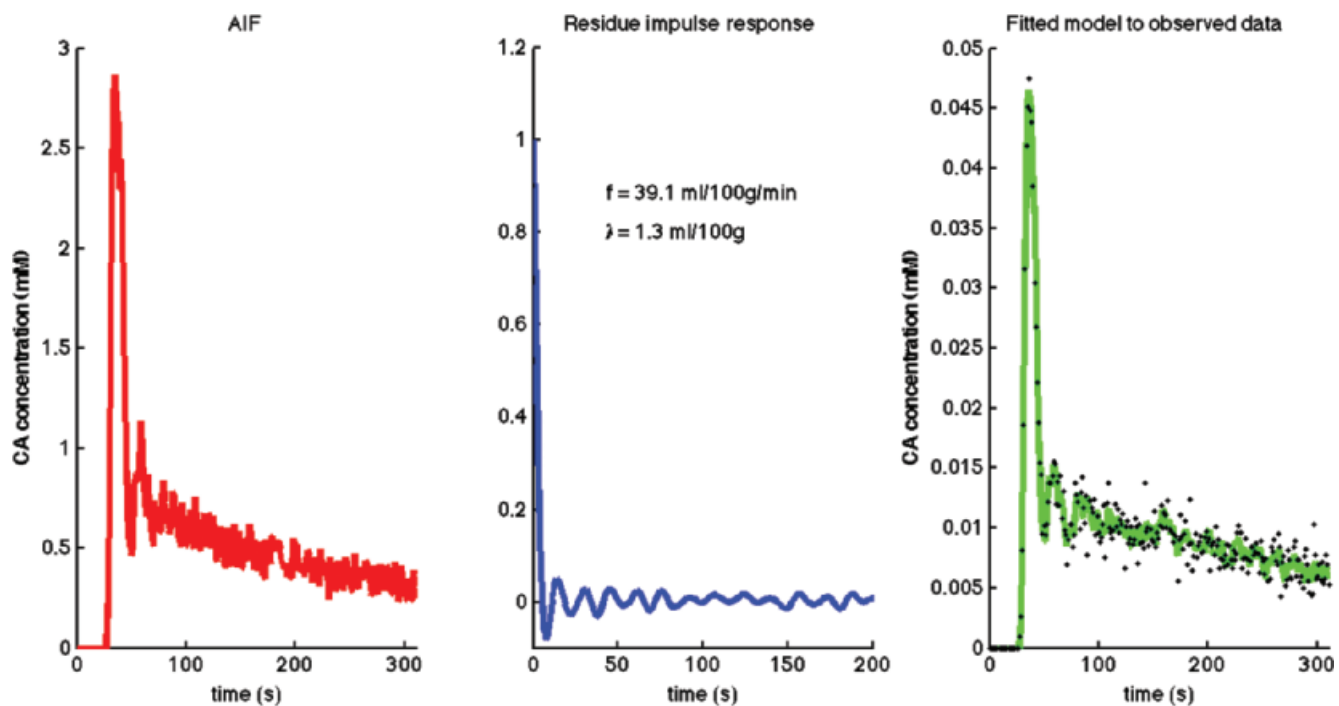


Figure 8-10. Example of the use of the generalized singular value decomposition (GSVD) with regularization using the *L*-curve method (see text). AIF and data are the same as in Figures 8.5 and 8.9. Note the reduction of the oscillations of the residue impulse response function, still fitting the data and no obvious underestimation of perfusion.

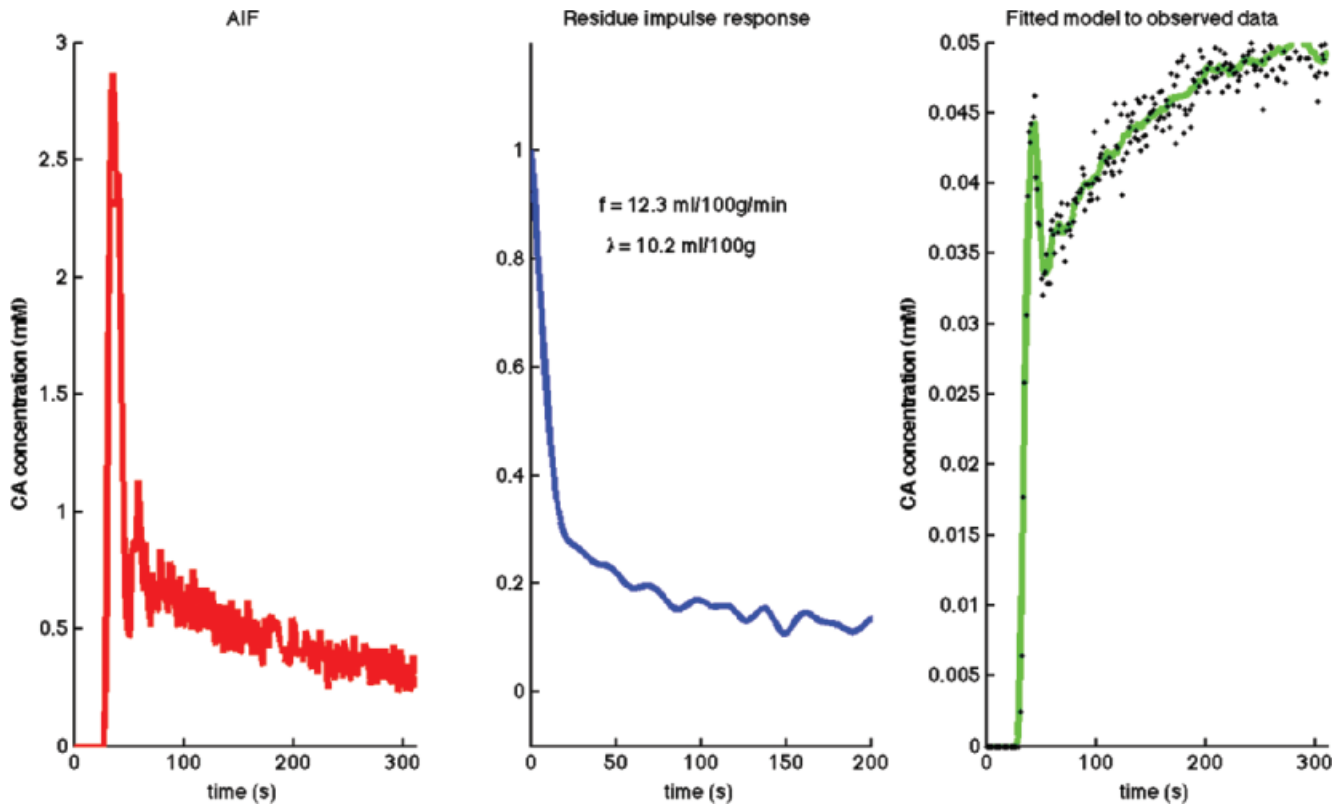


Figure 8-11. Example of the use of the generalized singular value decomposition (GSVD) with regularization using the L -curve method (see text). AIF and data are the same as in Figure 8.7. λ should be interpreted as the volume of distribution and corresponds approximately to the sum of v_b and v_e in Figure 8.7.

namely, that the RIF is a nonincreasing function. The “generalized singular value decomposition” (GSVD)^{40,41} seeks to find the solution from the minimization of

$$\min \left\{ \|\mathbf{A}\bar{x} - \bar{y}^{\text{obs}}\|^2 + \lambda^2 \|L(\bar{x})\|^2 \right\} \quad (26)$$

where L is the first derivative operator and λ is the degree of regularization. If λ is set to zero, the solution is not regularized, and the RIF may manifest these unphysiologic oscillations. If λ is set to a very high value, the solution, that is, the RIF, will become very smooth without oscillations. The optimum value of the regularization parameter, λ , is found using the curvature of the so-called L -curve, a heuristic approach: a trade-off between obtaining a smooth RIF and match between $\mathbf{A}\bar{x}$ and \bar{y}^{obs} ,⁴² and can be implemented as an automatic procedure voxel-wise. A practical implementation is given in reference.⁷ Even the GSVD with regularization, which tends to eliminate abrupt changes of the RIF, seems to underestimate perfusion in some situations (see ref.¹⁷). Examples of using the GSVD in order to estimate brain perfusion are shown in Figures 8.10 and 8.11. Figure 8.12 shows an example of voxel-wise calculation of CBF, creating CBF maps of the brain, and Figure 8.13 shows maps of permeability of a patient with a brain tumor.

In conclusion, it is possible to find a solution to the general tracer kinetic equation (Eq. (6)), without specifying a specific model with its associated analytical expression, but the solution is very noise sensitive, and one has to regularize the solution, by either cutting eigenvalues or incorporating a smoothing operator, with a possible impact on the shape of RIF and some underestimation of f .

Equation (25) involves sums of the form $C_a(i)\text{RIF}(j)\Delta t$, and the term represents an area of a square. If $C_a(i)$ or $\text{RIF}(j)$ are characterized by a pronounce change from sample to sample, then this discrete calculation will overestimate or underestimate the area compared to a convolution performed by a real continuous integration. This will introduce a bias of the resulting perfusion. In order to ameliorate this problem, one can either interpolate data to a finer temporal grid, for example, by a factor of 2 to 10, or use the trapezoid rule, and Eq. (25) will be given as²⁸

$$f \Delta t \begin{bmatrix} C_t(1) \\ C_t(2) \\ C_t(3) \\ \vdots \\ C_t(N) \end{bmatrix} = \begin{bmatrix} \frac{C_a(1)}{2} & 0 & 0 & \cdots & 0 \\ \frac{C_a(2)}{2} & \frac{C_a(1)}{2} & 0 & \cdots & 0 \\ \frac{C_a(3)}{2} & C_a(2) & \frac{C_a(1)}{2} & \cdots & 0 \\ \vdots & \vdots & \vdots & \ddots & \vdots \\ \frac{C_a(N)}{2} & C_a(N-1) & C_a(N-2) & \cdots & \frac{C_a(1)}{2} \end{bmatrix} \begin{bmatrix} \text{RIF}(1) \\ \text{RIF}(2) \\ \text{RIF}(3) \\ \vdots \\ \text{RIF}(N) \end{bmatrix} \quad (27)$$

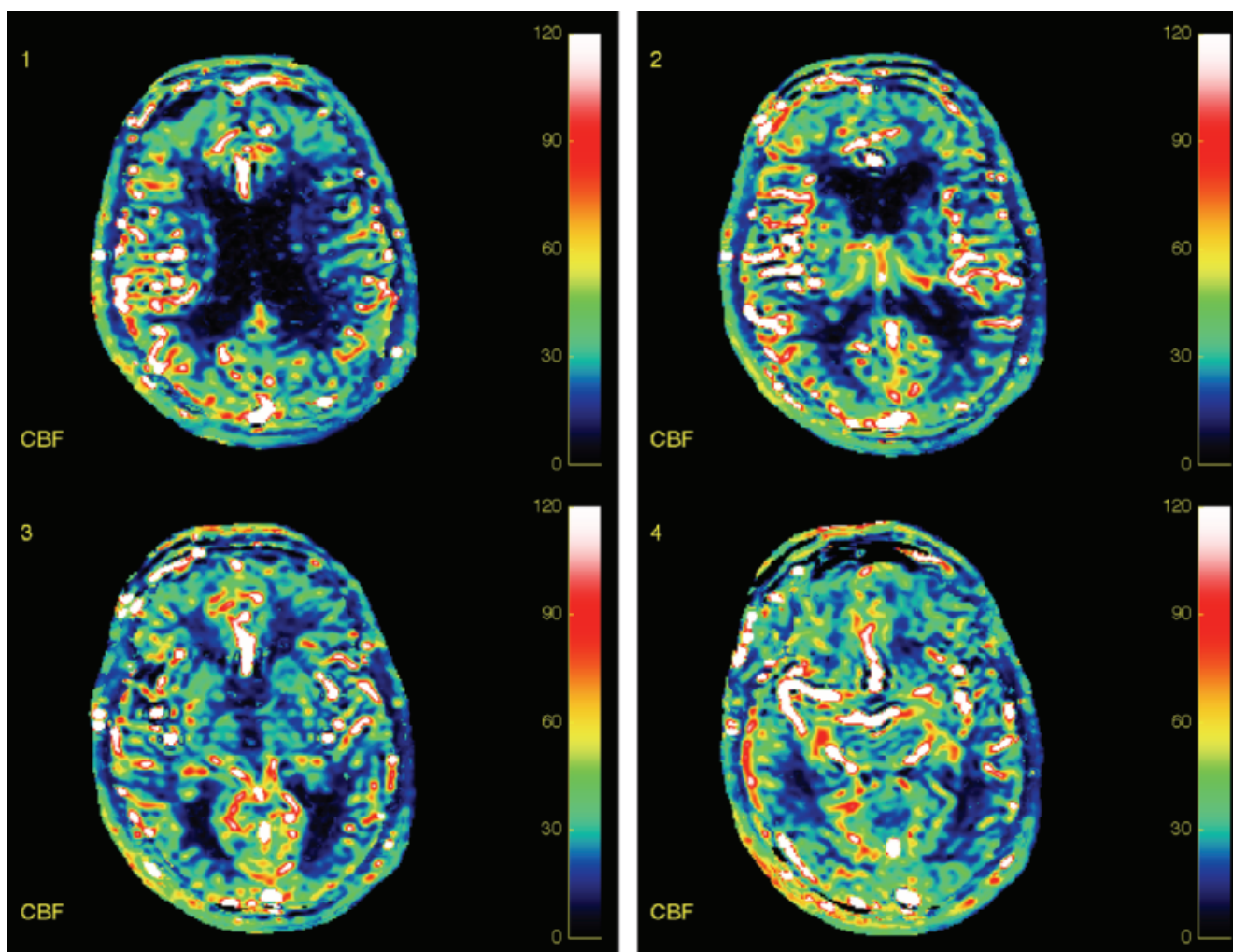


Figure 8-12. CBF maps using dynamic contrast-enhanced T₁-weighted MRI, at 3 T, using a saturation fast-field echo MR sequence, with a temporal resolution about 1 second. CBF is calculated pixelwise using the GSVD with *L*-curve regularization. Color scale is in mL/100 mL/min. The subject has a slight asymmetric perfusion pattern corresponding to cerebral media artery, with decreased perfusion corresponding to a known internal carotid stenosis at the same side.

■ The Arterial Input Function—Direct Measurement

The arterial input function, $C_a(t)$, represents the arterial concentration of the CA used as a function of time and is often abbreviated the AIF. It is necessary to measure or estimate the AIF if absolute physiologic measures of the tissue are wanted. The AIF can be obtained from arterially placed catheter, but it is more convenient if the AIF can be obtained from the dynamic images obtained during the bolus passage. For the heart, the left ventricle is a good location, and for the brain, the internal carotid artery (ICA) is obviously a good choice. Ideally, the AIF should be obtained from an artery as close as possible to the tissue in focus. If not, the AIF will be time shifted compared to the tissue enhancement curve, typically a couple of seconds ahead of the tissue. In all the models above, we have assumed simultaneous MR signal increase of tissue and arterial blood corresponding to the bolus arrival. If this condition is not satisfied, severe error of estimates of perfusion and transit times might be introduced. Therefore, the AIF should be shifted

accordingly before applying the tracer kinetic model, or the time shift can be incorporated in the model: $C_a(t - T_{lag})$. Thus, an additional parameter enters the model and has to be fitted along with the other free parameters of the model, hopefully with an improved fit and a significant reduction of the residual error of the fit. Another problem is that the shape of the AIF will also change as the CA passes through the vascular tree before entering the tissue in focus. Typically, the AIF entering to the tissue will look like a low-pass filtered (dispersed) version of the AIF measured at a long distance from the tissue in focus. This effect is probably small in normal tissue, but might become important in ischemic tissue with possible collateral vessel formation and long traveling distance. The importance of this problem has not really been assessed and is often ignored in the MR literature, but in nuclear medicine, the problem is treated by adding a filter function like $\exp(-t/T_{smooth})$ into the convolution kernel of Eq. (6), adding an additional parameter to be fitted. It should be realized that an error of the AIF directly propagates to the final result, and if the entire AIF is underestimated with a factor of 2, then perfusion is overestimated with a factor of 2.

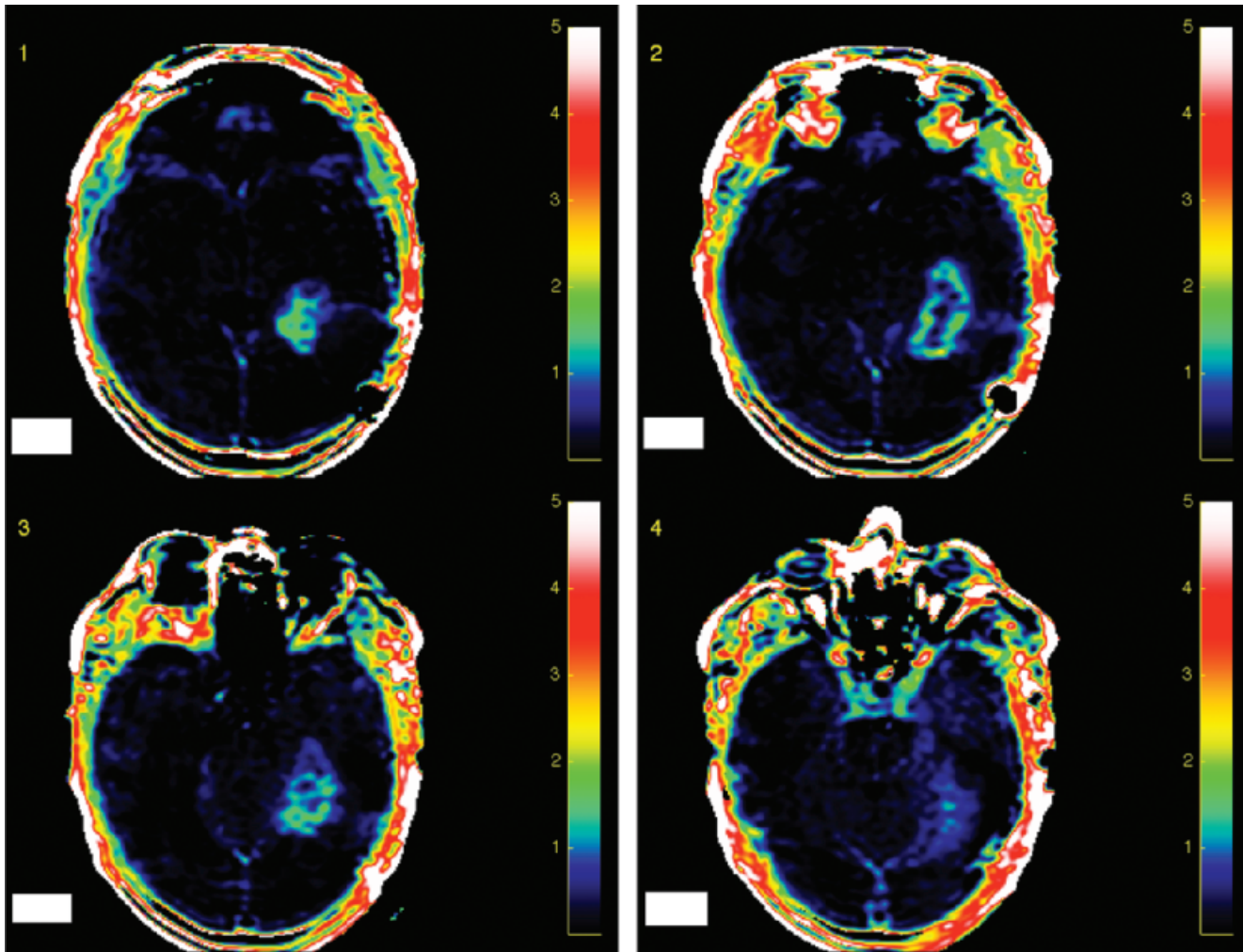


Figure 8-13. Maps of permeability (k_1) using dynamic contrast-enhanced T_1 -weighted MRI, at 3 T, using a saturation fast-field echo MR sequence, with a temporal resolution about 1 s. Permeability is calculated pixelwise using the Patlak method. Color scale is in mL/100 mL/min. The patient has an enhancing brain tumor and has previously been operated.

Schmitt et al.⁴³ showed in a computer simulation that the perfusion and the perfusion reserve could be underestimated with 50% and 20%, respectively, with an unaccounted dispersion of the AIF. Calamante et al.⁴⁴ showed a similar dependence on a delayed and dispersed AIF on CBF calculations.

The configuration of the AIF depends on factors as injection rate, central versus peripheral injection site, resistance in the pulmonary circulation, rest, or stress conditions. The peak and duration of the AIF are found to correlate with the function of the right and left ventricle.⁴⁵ Saline infusion after the bolus injection of CA may also effect the AIF configuration.⁴⁶ The AIF is also influenced by the concentration of CA, and injection rates between 2 and 10 mL/s have shown that the peak and width of AIF are significantly lower and broader for injection rates at 2 and 3 mL/s than for rates of 5 mL/s, but no difference was observed between the rates of 5 mL/s up to 7 and 10 mL/s.^{45,47} An obvious question is what is best? There is no real consensus on this matter, but a fast injection rate may probably be preferred, because of a more favorable contrast-to-noise ratio and improved RIF estimation especially in the brain because of a more clear distinction between tissue response and the AIF.

The temporal resolution used for obtaining the AIF should be high enough, in the order of seconds for the injection rate 1 to 10 mL/s; otherwise, the fine details of the AIF is missing, and especially

the peak concentration and the initial slope might be inaccurate due to undersampling of the curve. Figure 8.5 shows a typical AIF obtained from an ROI placed in the ICA of a human.

The AIF is quite unique from person to person and even from trial to trial within the same subject.⁴⁸ Therefore, the AIF should be estimated for each trial; a standardized population-based general AIF is not recommendable and should be avoided.

■ The Arterial Input Function—Correction for a Partial Volume Effect

From the above discussion, we see that the AIF should be obtained as close as possible to the tissue in focus. This can some time be accomplished by choosing a small artery. However, as a consequence, this artery will likely suffer from a partial volume effect, which means that the voxels in the ROI will consist of a mixture of tissue and blood in the artery, thus a partial volume effect, and the arterial concentration will be underestimated. This situation is aggravated by the fact that we often want to run a dynamic MR sequence with a high time resolution, meaning that we have to sacrifice the spatial resolution, that is, reduce the matrix size. The consequence is a considerable point spread function, meaning a

blurring of a small artery and additional underestimation of the arterial input function. In addition, the AIF can suffer from pulsation artifacts, probably related to an inflow effect, but is otherwise not rigorously characterized in the literature. One simple way to assess the partial volume effect is to look at a profile of the vessel as a function of the spatial resolution and note when a plateau occurs inside the vessel. In the left ventricle of the heart, this is easily obtained with conventional spatial resolution, but often, such a resolution in smaller vessels is not compatible with the timing requirement, for example, in the brain.

Sometimes, it is possible to correct for the partial volume effect. The brain has a large draining venous system, and especially, the sagittal sinus has a larger lumen compared to the brain arteries including ICA. Conservations of mass tell us that for an organ with one inlet (artery) and one outlet (vein), the AIF and the venous outflow function (VOF) should have the same area. Thus, matching the area of the AIF with the area of the VOF will mitigate, although not eliminate the partial volume effect if the vein also suffers from some degree of partial volume effect. It has been shown that this method has some value in the brain using ICA and the sagittal sinus.⁴⁹ In fact, due to the BBB, the AIF and VOF are almost identical, and therefore a scaling of the AIF and a time shift of the VOF will create a nearly perfect match of the two functions, which also signify that dispersion through the normal brain tissue is minimal (see Fig. 8.14). It should be remembered that also the basilar artery subserves blood to the brain, and the sagittal sinus blood flow constitutes about 50% of the total effluent blood from the brain.

Elimination of a possible partial volume effect from the sagittal sinus can be taken one step further, using the phase information. The

following is based on the study of van Osch, originally developed for dynamic susceptibility contrast-enhanced perfusion imaging,⁵⁰ but is here adapted for DCE T₁ perfusion imaging of the brain, and further simplified, and thus easily implemented.

Using the modulus of the MR signal, the general relationship between the MR signal and concentration of a paramagnetic CA in the blood is $S(t) = f(M_0, TR, TE, TD, \alpha, r_1, R_1^b, C_{\text{mod}}(t))$, where $S(t)$ is modulus MR signal, t is time, f describes the MR sequence function, M_0 is a constant related to the equilibrium magnetization, TR is the repetition time, TE is echo time, α is the flip angle of the readout pulses, r_1 is the relaxivity, and R_1^b is the blood longitudinal relaxation rate before arrival of the CA. Here, we illustrate the implementation using a simple fast-field MR sequence with a non-selective 90-degree prepulse preceding the first α -pulse by a time period of TD, with central phase-encoding scheme, and spoiling between lines in k-space. So for this particular sequence, the relationship is simply

$$S(t) = M_0 \left(1 - e^{-TD(R_1^b + r_1 C_{\text{mod}}(t))} \right) \quad (28)$$

In practice, M_0 and R_1^b are measured before contrast injection, and M_0 also includes regional variation due to B_0 inhomogeneity; B_1 inhomogeneity, that is, $\sin(\alpha)$; and a T_2^* decay term, which we consider minimal. Having measured R_1^b and M_0 before contrast injection, it is easy to find $C_{\text{mod}}(t)$, from the modulus of the MR signal.

The blood concentration can also be estimated from the phase of the MR signal.⁵¹ Especially for a long tube placed parallel with the B_0 field containing a paramagnetic CA, the relationship between the

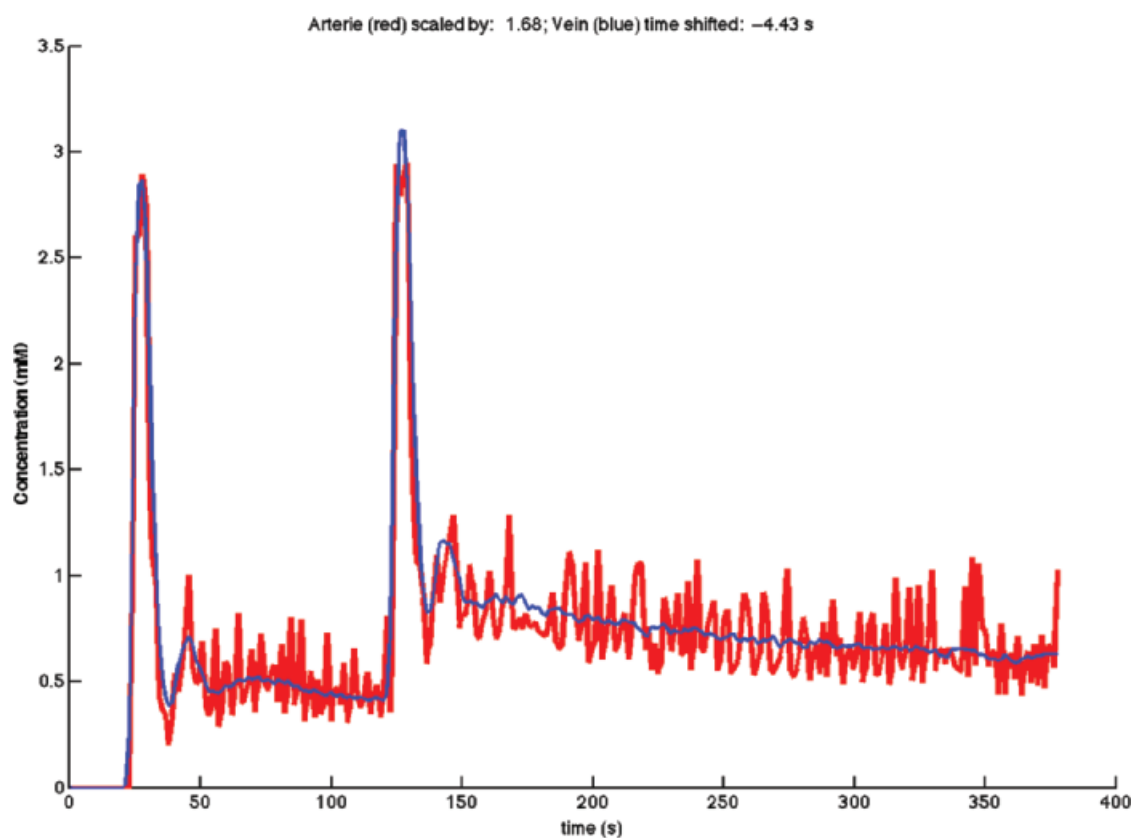


Figure 8-14. The AIF (*red*) is obtained from the internal carotid artery; the venous curve (*blue*) is obtained from the sagittal sinus. Fitting of the curves is provided by scaling the AIF, while the venous curve is time shifted back in time. In this case, two separated bolus injections, each of half dose, are administered. Note that the AIF suffers from what is believed to be inflow effects, which are completely absent from the venous curve.

phase change as a function of time ($\Delta\Phi(t)$) and concentration as a function of time ($C_{\text{phase}}(t)$) is

$$\Delta\Phi(t) = \frac{2}{3} \pi \text{TE} \gamma B_0 \chi_m C_{\text{phase}}(t) \quad (29)$$

where γ is the proton gyromagnetic ratio (4.258×10^7 Hz/T), B_0 is the magnitude of the main magnetic field in tesla, and χ_m is the molar susceptibility of the CA (3.4×10^{-7} mM $^{-1}$). The sagittal sinus constitutes nearly a long tube, and one can always find portions, which run parallel with the B_0 field, and in addition, transversal imaging of the brain allows such a portion to be imaged during a perfusion study. If the complex MR signal is obtained, then one can calculate the concentration from either Eqs. (28) or (29), and if no interfering factors exist, then $C_{\text{phase}}(t) = C_{\text{mod}}(t)$. As shown later, $C_{\text{phase}}(t)$ is not equal to $C_{\text{mod}}(t)$, most likely because $C_{\text{mod}}(t)$ is affected by a partial volume effect. $C_{\text{phase}}(t)$ is less susceptible to the effect of the partial volume, but suffers from poor signal to noise and is bias especially for low concentration as shown later.

In order to solve this problem, we consider an ROI placed over the sagittal sinus and having a fraction containing blood (v_b) and a complementary fraction containing tissue (v_t), where $v_t + v_b = 1$. In addition, we assume that these two tissue fractions behave as a two-compartment system without any water exchange (see later). Therefore, the complex MR signal for this ROI is

$$S(t) = v_t M_0 \left(1 - e^{-\text{TD} R_t^i}\right) e^{i\Phi_t} + v_b M_0 \left(1 - e^{-\text{TD}(R_t^i + r_i C_{\text{mod}}(t))}\right) e^{i(\Phi_b + \Delta\Phi(t))} \quad (30)$$

where Φ_b and Φ_t are initial phase of the blood and tissue component in an ROI, respectively. R_t^i is the longitudinal relaxation rate of the tissue component.

Before arrival of the CA, we just have

$$S(0) = v_t M_0 \left(1 - e^{-\text{TD} R_t^i}\right) e^{i\Phi_t} + v_b M_0 \left(1 - e^{-\text{TD} R_t^b}\right) e^{i\Phi_b} \quad (31)$$

$S(0)$ is an average of all baseline points before arrival of the CA. Therefore, the baseline-subtracted complex MR signal during the bolus passage is

$$S(t) - S(0) = v_b M_0 \left(1 - e^{-\text{TD}(R_t^b + r_i C_{\text{mod}}(t))}\right) e^{i(\Phi_b + \Delta\Phi(t))} - v_b M_0 \left(1 - e^{-\text{TD} R_t^b}\right) e^{i\Phi_b} \quad (32)$$

This equation contains two unknown: v_b and Φ_b . If these were known, $C_{\text{mod}}(t)$ can be calculated from

$$\left\| S(t) - v_t M_0 \left(1 - e^{-\text{TD} R_t^i}\right) e^{i\Phi_t} \right\| = \left\| S(t) - S(0) + v_b M_0 \left(1 - e^{-\text{TD} R_t^b}\right) e^{i\Phi_b} \right\| = v_b M_0 \left(1 - e^{-\text{TD}(R_t^b + r_i C_{\text{mod}}(t))}\right) \quad (33)$$

and $C_{\text{phase}}(t)$ can be calculated from

$$\arg \left[S(t) - S(0) + v_b M_0 \left(1 - e^{-\text{TD} R_t^b}\right) e^{i\Phi_b} \right] - \Phi_b = \frac{2}{3} \pi \text{TE} \gamma B_0 \chi_m C_{\text{phase}}(t) \quad (34)$$

For correct values of v_b and Φ_b , $C_{\text{phase}}(t) = C_{\text{mod}}(t)$. As v_b and Φ_b are unknown, we use $\sum (C_{\text{phase}}(t) - C_{\text{mod}}(t))^2$ as a cost function to be minimized in a fitting procedure searching for the most optimal v_b and Φ_b .

■ The Arterial Input Function—Optimization of Dose

The T_1 -weighted MR sequences typically used in DCE imaging include a prepulse, which is either an inversion or saturation pulse. The MR signal range is typically much higher for the AIF compared with the tissue MR signal increase. Because of the low

tissue response, it is preferable to use a high dose of CA and an MR sequence optimized for high sensitivity, for example, long inversion time (TI). However, this may cause truncation and underestimation of the AIF due to full magnetic recovery in the blood pool. This means an artificial underestimation of the AIF and may lead to substantial errors in calculation of tissue perfusion.⁵² High concentrations of gadolinium-DTPA in the blood pool may also reduce the signal due to T_2^* effects,⁵³ and obviously, the shortest allowed echo time should be used, which will eliminate or at least minimize the T_2^* effect. The use of a double-echo sequence with short echo times might rule out and correct for a possible T_2^* effect. Careful optimization and validation is therefore required, ensuring that both the AIF and the tissue signal during the bolus passage are measured correctly within the dynamic range of the entire system. If this is not possible, the dual-bolus approach,^{54,55} the prebolus technique,⁵⁶ or the dual-imaging sequence^{52,57} through repeated measurements of the bolus passage using low and high doses of CA focusing on the AIF and the tissue response, respectively, is a possibility.

■ The Arterial Input Function—Indirect Measurement

Obtaining an AIF can be a challenge and is subjected to many potential errors as just explained, and sometimes, no artery is available in the field of view or close to the tissue of interest. Therefore, methods for estimating the AIF without directly measuring the AIF, so-called blind estimation of the AIF, are of considerable interest. Several methods have been suggested, but only two principal methods, the multiple reference tissue-based AIF method^{58,59} and jointly estimated AIF seems of relevance. The starting point for these methods is the recognition that the equation $\vec{y} = f \Delta t A \vec{x}$ represents N linear equations, because we have N samples. Furthermore, let the entries of \vec{x} be specified by an analytic model, for example, having three free parameters depending on the actual model used. In the situation where AIF is missing, we have $N + 3$ unknown, which cannot be estimated. If we obtain information from multiple tissue ROIs, including ROIs placed in pathologic tissue, preferably with a large diversity of the physiologic tissue parameters between sites, and we assume that R tissue sites are exposed to the same AIF (except for a possible difference of arrival time, which also can be incorporated), then the number of equations is RN , but the number of unknown is only $N + 3R$. Therefore, in principle, enough information is available in order to estimate the matrix \mathbf{A} (the AIF with N samples). In the multiple reference tissue-based AIF method, the AIF is estimated without assuming a specific form of the AIF, and the physiologic tissue parameters from all tissue sites are estimated in conjunction with the AIF. The estimation of the AIF and the other unknown physiologic constants are based on ingenious and fast optimization procedure, minimizing the residual error of the fit. The method does not provide an absolute scale of the AIF, and consequently, the physiologic parameters are estimated only within a scale factor (except time constants as K_i/V_e). Scaling of AIF can be provided from incorporating, for example, a literature value of the interstitial space of the tissue, or from a real single measurement of the blood concentration of the CA during the late phase of the bolus passage, where the CA is well mixed in the entire blood pool, and saturation, arrival time, and temporal resolution are minor problems. The obtained blind estimated AIF can then be used to calculate the physiologic tissue parameters voxel-wise.

The jointly estimated AIF utilized a parameterized form of the AIF. Previous models based on a mono-, bi-, or triexponential AIF are not accurate enough. Instead, a superposition of 2 to 3 normalized gamma-variate functions and a Gaussian or sigmoid functions with about 10 to 15 adjustable free parameters seem to model

the measured AIF encountered in vivo.⁶⁰ Thus, the total number of free parameters is considerable reduced compared with the multiple reference tissue-based AIF method and consequently alleviate the requirement of inclusion of multiple reference tissue sites, assumed to have the same AIF. However, multiple tissue enhancement curves, randomly selected within a particular tissue type, for example, within tumor tissue, is still necessary and assumed to have the same (local) AIF, in order to tune the free parameters of the AIF.⁶¹ As with the multiple reference tissue-based AIF method, a model of the RIF is still required, and the tissue physiologic parameters are fitted simultaneously. Like the multiple reference tissue-based AIF method, the AIF and the physiologic parameters of the tissue are only determined within a scale factor, and a final scaling is still necessary.

The importance of blind estimation of the AIF resides in the fact that it provides a possibility of finding and utilizing a local AIF, incorporating a possible dispersion, and it alleviates the inherent problems mentioned above, thus obtaining a more accurate AIF for the given tissue site. It has been shown that local dispersion of the AIF can have a significant impact on the results obtained⁶² and that the local AIF in normal brain tissue deviates significantly from the local AIF in an adjacent brain tumor. The danger is that using algorithms for obtaining a local AIF, which is based on only a local set of tissue enhancement curves, results in mixing characteristics of the local AIF and the tissue enhancement curves, and thus the results will be biased. However, the finding of a significant reduction of the residual error of the fit to tumor data, when using the local blind estimated AIF from tumor tissue, compared to a local blind estimated AIF from normal tissue, suggests a real improvement of accuracy.⁶³

Blind estimation of the AIF necessitates a model of the RIF, and so far, only the extended Tofts model has been used in DCE T₁-weighted studies. Future research is needed for investigate blind AIF estimation in conjunction with other models. In conjunction with dynamic susceptibility-weighted perfusion imaging, it has been shown that a blind local AIF can be obtained when using independent component analysis, without the need of specifying a model for the RIF,⁶⁴ a method that also should be exploited for DCE T₁-weighted studies.

■ Linking Tracer Kinetic Theory and Modeling to MRI

Tracer kinetic modeling seeks to describe the biologic systems handling of the CA and works directly on CA concentration. In DCE T₁-weighted MRI, information about the CA is via the MR signal, and the signal is generally a nonlinear function of the CA concentration. This is because the MR signal is bound to the magnetization in the voxel, and the magnetization spans from $-M_0$ to $+M_0$, where M_0 is the equilibrium magnetization. The CA considered here works by enhancing the longitudinal relaxation rate R_1 ($=1/T_1$; the reciprocal of the longitudinal relaxation time T_1) of water protons preferably by binding to the paramagnetic core of the CA, so-called inner sphere relaxation. A smaller contribution comes from the so-called outer sphere relaxation, based on proximity between the paramagnetic core and the water protons.^{65,66} The relaxation mechanism is governed by the large magnetic dipole moment associated with the unpaired electrons in the inner electron shells of the paramagnetic atoms through an electron–nuclear dipolar interaction. The associated large dipole creates an oscillating magnetic field with a broad frequency distribution, including frequencies at the relevant Larmor frequency, inducing relaxation. Because of a fast exchange between bound and free water, the relaxation enhancing effect is transmitted to the entire water population.^{65,66} The enhanced T₁ relaxation results in an MR signal increase when using a T₁-weighted MR sequence.

It is important to realize that the effect of a CA, when using a T₂*-weighted MR sequence can provide relaxation due to the electron–nuclear dipolar interaction, but also indirectly over a much longer distance due to creation of local magnetic field inhomogeneity, a susceptibility effect, without direct contact with the paramagnetic core of the CA. The MR signal decreases during the bolus passage when using a T₂- or T₂*-weighted MR sequence, because R_2 ($=1/T_2$) and R_2^* ($=1/T_2^*$) increase. The most often used paramagnetic atom is gadolinium (Gd) belonging to the lanthanide series of chemical elements with the atomic number 64 (¹⁵⁸gadolinium(III) is the most abundant and stable isotope). Both theoretical and experimental studies have shown that for a homogeneous water solution of the normally used MRI CAs, a linear relationship exists between the CA concentration and the longitudinal relaxation rate:

$$\frac{1}{T_1^{CA}} = \frac{1}{T_1} + r_1 C \Leftrightarrow R_1^{CA} = R_1 + r_1 C \Leftrightarrow \Delta R_1 = r_1 C \quad (35)$$

where T_1^{CA} and T_1 are the relaxation times with and without CA, r_1 is the relaxivity defined as the change in the longitudinal relaxation rate per concentration unit of the CA (mM s^{-1}), and C is the concentration of the CA. The relaxivity depends on field strength and the type of CA. Paramagnetic metals, as Gd is toxic, and toxicity is eliminated by chelation with a molecule, for example, diethylenetriamine pentaacetic acid (Gd-DTPA), which secures a fast clearance by the kidney. In general, the size and configuration of the molecule, the number of paramagnetic atoms, and water accessibility to the paramagnetic core determine the relaxivity. A pertinent question is how dependent the relaxivity is on the local biologic tissue environment. In a comprehensive study, Donahue et al. measured the relaxivity in saline, plasma, and cartilage and found a relaxivity of about 4 (mM s^{-1}) for Gd-DTPA.⁶⁷ Neither changing the plasma protein concentration nor compression of the cartilage (reducing the water content) nor trypsinization of the cartilage (nearly completely removing proteoglycan and fixed charges) had significant effect on the relaxivity. At a field strength of 1 T, the relaxivity was about 20% higher compared to field strength of 4.7 and 8.5 T. Many have measured the relaxivity of Gd-DTPA in biologic tissues, for example, the relaxivity of blood plasma is 3.9 ± 0.2 (mM s^{-1})⁶⁸ and 4.3 (mM s^{-1}) in the myocardium at 1.5 T.⁶⁶ The relaxivity is generally assumed to be independent of the biologic microenvironment, but exceptions might occur.

The MR signal equation derived from the Bloch equation corresponding to the actual MR sequence used provides the link between the MR signal and the concentration of the CA. A relevant example is imaging using 2D fast gradient echo sequence (GRE sequence), with a nonselective 90-degree prepulse, followed by repeated slice-selective readout α -pulses (flip angle 10 to 30 degrees), each separated by a TR of a few milliseconds. The time between the prepulse and the first α -pulse is called TD. The MR signal equation becomes very simple if centric phase encoding is used, meaning that the first phase-encoding step corresponds to the center of K -space ($K_y = 0$, phase-encoding gradient is zero). TE should be as short as possible and preferably below 1 milliseconds, so T₂*-weighing can be ignored. Residual transverse magnetization should be spoiled effectively by, for example, rf and gradient spoiling before the next α -pulse. The signal equation is then

$$S = S_0 \sin(\alpha) (1 - \exp(-TDR_1)) \quad (36)$$

where S is the MR signal, S_0 is the maximal MR signal, and R_1 is the relaxation rate without any CA. S_0 is a constant and proportional to proton density, receiver gain, and the local coil sensitivity. The time resolution can be as high as 0.5 seconds, depending on matrix size and number of slices. Generally, the MR signal is primarily determined by the phase-encoding step corresponding to the “zero phase-encoding step” ($K_y = 0$), because this step is the most

important determinant for the overall signal strength. In contrast to nuclear medicine measurements, where sampling of radioactive counts is more uniform over the sampling interval, the level of the MR signal is determined at a distinct point in time, corresponding to traversal of the center of K -space. In the present context, Eq. (36) is a function of position (the voxel), time, and CA concentration. Focusing on time and concentration, the equation becomes

$$S(t) = S_0 \sin(\alpha) \left(1 - \exp(-TD(R_1 + r_1 C(t))) \right) \quad (37)$$

If we obtain measurements of $S_0 \sin(\alpha)$ (taken as one constant) and R_1 before CA injection, and assume a known value of r_1 , then $S(t)$ can easily be converted to $C(t)$. $S_0 \sin(\alpha)$ and R_1 can be obtained by a regular T_1 measurement by stepping through a set of TD values and measure the corresponding signal. Note that $S_0 \sin(\alpha)$ obtained voxel-wise corrects for scanner inhomogeneity and nonuniform flip angle. The nonselective 90-degree prepulse should be as accurate as possible, for example, using an adiabatic pulse, and coverage should be large in order to label blood entering the field of view. In all perfusion imaging, it is important to obtain a reliable baseline signal before CA enters the tissue, for example, 10 to 20 samples. If we call the average baseline signal $\hat{S}(0)$, then Eq. (37) can be expressed as

$$\frac{S(t) - \hat{S}(0)}{\hat{S}(0)} = \frac{1 - \exp(-TD r_1 C(t))}{\exp(TD R_1) - 1} \quad (38)$$

If TD is short, we may use the approximation $\exp(x) \approx 1 + x$ ($x < 0.2$) and get

$$\frac{S(t) - \hat{S}(0)}{\hat{S}(0)} \approx \frac{r_1 C(t)}{R_1} \quad (39)$$

This equation shows that the relative MR signal change is linearly related to the CA concentration, if the argument of the exponential function is small. For this reason, some people are using a very low dose of CA, to secure linearity. If in addition R_1 is assumed and fixed at a value, the concentration can be estimated without the initial T_1 measurement. However, assuming a fixed T_1 value has lately questioned as a valid simplification for body imaging.⁶⁹ It should also be noted that if $\hat{S}(0)$ is close to zero, the relative MR signal change may be very sensitive to noise of the baseline MR signal.

If centric phase encoding is impossible, one has to take all phase-encoding steps and the corresponding manipulation of the magnetization into account until the center of K -space is reached. Note that for short TR of a few milliseconds, the longitudinal magnetization evolves during traversal of K -space. If the center of K -space is reached after n phase-encoding steps, Eq. (37) becomes⁷⁰

$$S(t) = S_0 \sin(\alpha) \left[\left(1 - e^{-TD(R_1 + r_1 C(t))} \right) \left(\cos(\alpha) e^{-TR(R_1 + r_1 C(t))} \right)^{n-1} + \left(1 - e^{-TR(R_1 + r_1 C(t))} \right) \frac{1 - \left(\cos(\alpha) e^{-TR(R_1 + r_1 C(t))} \right)^{n-1}}{1 - \cos(\alpha) e^{-TR(R_1 + r_1 C(t))}} \right] \quad (40)$$

Retrieval of $C(t)$ can be provided by an iterative process. The flip angle should either be known or, alternatively, can be estimated together with $S_0 \sin(\alpha)$ and R_1 from the T_1 measurement voxel-wise before CA injection. Again, the 90-degree prepulse should be as accurate as possible.

If the 90-degree prepulse is not perfect, or the 90-degree prepulse is replaced by a 180-degree inversion pulse, then longitudinal magnetization survives from one frame to the next, the evolution of the magnetization from the last α -pulse of a frame to the prepulse of the next frame has to be taken into account, and the MR signal equation becomes more sophisticated.⁷¹ When taking the history of the magnetization into account, steady-state MR signal equations are normally calculated and used, that is, the MR signal initially shows some oscillation and gradually settles at a constant

steady-state value. As an example, an often used MR sequence in DCE T_1 -weighted imaging is a 3D spoiled T_1 -weighted gradient echo sequence. The TE is short, preferably a few milliseconds, but TR is typically around 100 milliseconds, separating each readout α -pulses. The magnetization before each α -pulse is in steady state (have the same size), in contrast to the previously mentioned fast gradient echo sequences. Such a 3D sequence provides better coverage (slice direction) and better in-plane spatial resolution, and possible better signal-to-noise ratio than do corresponding 2D sequences, sacrificing the temporal resolution, which often is no better than 2 to 3 seconds and often 5 to 10 seconds. The steady-state MR signal equation, assuming negligible T_2^* contribution, corresponding to the center of K -space is

$$S(t) = S_0 \sin(\alpha) \frac{1 - e^{-TR(R_1 + r_1 C(t))}}{1 - \cos(\alpha) e^{-TR(R_1 + r_1 C(t))}} \quad (41)$$

Again, $C(t)$ can be estimated if $S_0 \sin(\alpha)$, R_1 , and the flip angle is known. $S_0 \sin(\alpha)$ and R_1 can be estimated before CA injection by varying either TR or the flip angle. A pertinent question is whether a steady-state signal equation can be used during the bolus passage where the longitudinal relaxation rate changes due to the concentration changes. According to own unpublished simulations, no major error is introduced in this situation. However, it is possible to follow the magnetization from frame to frame during the bolus passage of the CA without relying on a steady-state equation.⁷⁰

In conclusion, there is a linear relationship between the CA concentration and change in the longitudinal relaxation rate. The MR signal can be converted to concentration by use of the relevant MR signal equation. It is important to optimize the MR sequence parameters, for example, a long TI or TD is beneficial for improving sensitivity, but in conjunction with a high dose of CA, there is a risk of getting full relaxation of the MR signal, especially with regard to the AIF, which will suffer from truncation and therefore result in an overestimation of the physiologic parameters.

Water Exchange

Biologic tissue contains several compartments, such as plasma, erythrocytes, extravascular extracellular space (interstitial space), and the intracellular space. The CA distribution is often uneven and depends on concentration, permeability of the capillary membranes, cellular membranes, and time for equilibration among other factors. In DCE T_1 -weighted MRI, the effect of the CA in a compartment can affect an adjacent compartment without any CA, if a significant water exchange between the two compartments occurs. In fact, the rate of water exchange between compartments influences the overall tissue relaxation. This complicates matters but also opens for the possibility of measuring water permeability.

The water exchange can be categorized into four types: fast, intermediate, slow, and no-exchange regime.⁷² The *fast*-exchange regime between compartments a and b with relaxation times T_1^a and T_1^b is characterized by

$$\frac{1}{\tau} \gg \left| \frac{1}{T_1^a} - \frac{1}{T_1^b} \right| = |R_1^a - R_1^b| \quad (42)$$

where

$$\frac{1}{\tau} = \frac{1}{\tau^a} + \frac{1}{\tau^b}$$

and τ^a and τ^b represent the mean lifetime of a proton in compartments a and b, respectively. This equation states that the water exchange frequency is much faster than the difference between the two compartments' intrinsic relaxation rates, that is, if each compartment's

relaxation rate were measured separately. In this case, the overall relaxation rate will be⁷³

$$R_1 = \nu^a R_1^a + \nu^b R_1^b \quad (43)$$

where ν^a and ν^b are the relative fraction of water of the two compartments ($\nu^a + \nu^b = 1$). The two compartments relax with one relaxation rate, and the relaxation process is monoexponential. Imagine that a CA is added to compartment b with concentration C . Then, still assuming fast exchange (could potentially move out of the fast-exchange regime; see later), the overall relaxation rate is

$$R_1^{CA} = \nu^a R_1^a + \nu^b (R_1^b + r_1 C^b) = \nu^a R_1^a + \nu^b R_1^b + \nu^b r_1 C^b = R_1 + \nu^b r_1 C^b$$

Now, defining an average CA concentration for both compartments as

$$\hat{C}(\nu^a + \nu^b) = \hat{C} = \nu^b C^b$$

results in

$$R_1^{CA} = R_1 + r_1 \hat{C} \quad (44)$$

This equation shows that even though the CA is nonuniformly distributed, the system behaves as if the CA is well mixed in both compartments, and the system relax monoexponentially, and a T_1 measurement before and after adding the CA will result in a concentration estimate corresponding to an even distribution of the CA in the two compartments. An important example is estimation of the CA concentration in arterial blood in conjunction with AIF measurement. It is generally accepted that the water exchange between plasma and the interior of the erythrocytes is very fast, with an exchange rate of 100 Hz.^{74,75} Even with a plasma concentration up to 6 mM as has been observed,⁶ the fast-exchange regime prevails. This means that an estimate of the CA concentration in blood, for example, in conjunction with measurement of the AIF, results in an estimation of the full blood concentration, even though the CA is confined to the plasma. The real plasma concentration can then be calculated from $C_a^p = C_a / (1 - \text{Hct}_{LV})$ where C_a^p and C_a are arterial plasma concentration and full blood concentration, respectively. In tracer kinetic equations, it is often convenient to use the real physiological concentrations and only later change concentration reference.

The no-exchange regime means no exchange of water between compartments. In this case, each compartment has its own distinct relaxation process, and the combined relaxation is multiexponential. If two compartments a and b have relaxation rate R_1^a and R_1^b , respectively, then the MR signal for a simple saturation recovery sequence with centric phase encoding becomes

$$S = S_0 \nu^a (1 - e^{-\text{TR} R_1^a}) + S_0 \nu^b (1 - e^{-\text{TR} R_1^b}) \quad (45)$$

Adding a CA to compartment b will change the relaxation rate of only that compartment, and the concentration can be measured by carefully measuring the biexponential relaxation process:

$$S^{CA} = S_0 \nu^a (1 - e^{-\text{TR} R_1^a}) + S_0 \nu^b (1 - e^{-\text{TR}(R_1^b + r_1 C^b)}) \quad (46)$$

If compartment a represents the extravascular space and b the vascular space, and we assume no exchange between these compartments, then the vascular space can be estimated from the ratio of total tissue MR signal change to the blood MR signal change before and after adding the CA⁷⁶:

$$\nu^b = \frac{\Delta S}{\Delta S^b} = \frac{S^{CA} - S}{\Delta S^b} \quad (47)$$

where ΔS^b is determined from a blood sample or from an ROI with pure blood placed within the vessel. This is quite distinct from

assuming a fast exchange between blood and the extravascular space. In this situation, we would have⁷⁶

$$\nu^b = \frac{C_t}{C_a} = \frac{\Delta R_1^t / r_1}{\Delta R_1^a / r_1} = \frac{\Delta R_1^t}{\Delta R_1^a} \quad (48)$$

assuming the same relaxivity for blood and tissue, as is normally done. Here, we also assume a fast exchange between the interstitial space and the intracellular water in both situations.

The slow exchange regime is defined as⁷²

$$\frac{1}{\tau} \ll \left| \frac{1}{T_1^a} - \frac{1}{T_1^b} \right| = |R_1^a - R_1^b| \quad (49)$$

In this situation, each compartment's relaxation rate will be modified as

$$\begin{aligned} \bar{R}_1^a &= R_1^a + \frac{1}{\tau^a} \\ \bar{R}_1^b &= R_1^b + \frac{1}{\tau^b} \end{aligned}$$

where τ^a and τ^b represent the mean lifetime of a proton in compartments a and b, respectively. The intermediate water exchange regime⁷⁷ is

$$\frac{1}{\tau} \approx \left| \frac{1}{T_1^a} - \frac{1}{T_1^b} \right| = |R_1^a - R_1^b| \quad (50)$$

Hazlewood has developed a two-site exchange model, which deals with the water exchange in general.⁷⁸ The model takes into account the combined relaxation and exchange of magnetization between compartments. For two compartments a and b, the model is given by the two coupled differential equations:

$$\begin{aligned} \frac{dM^a(t)}{dt} &= \frac{M_0^a - M^a(t)}{T_1^a} - \frac{M^a(t)}{\tau^a} + \frac{M^b(t)}{\tau^b} \\ \frac{dM^b(t)}{dt} &= \frac{M_0^b - M^b(t)}{T_1^b} - \frac{M^b(t)}{\tau^b} + \frac{M^a(t)}{\tau^a} \end{aligned} \quad (51)$$

Conservation of matters implies $M_0^a / \tau^a = M_0^b / \tau^b$ and $M_0^a + M_0^b = 1$. The solution is then given by

$$\begin{aligned} M^b(t) &= P_1 e^{\psi t} + P_2 e^{\phi t} + M_0^b \\ M^a(t) &= P_3 e^{\psi t} + P_4 e^{\phi t} + M_0^a \\ \Psi &= -\frac{1}{2} (k_1 + \sqrt{k_1^2 - 4k_2}) \\ \Phi &= -\frac{1}{2} (k_1 - \sqrt{k_1^2 - 4k_2}) \\ k_1 &= \frac{1}{T_1^a} + \frac{1}{\tau^a} + \frac{1}{T_1^b} + \frac{1}{\tau^b} \\ k_2 &= \frac{1}{T_1^a T_1^b} + \frac{1}{T_1^a \tau^a} + \frac{1}{T_1^b \tau^b} \end{aligned} \quad (52)$$

The amplitude P_1 to P_4 depends on the initial conditions, and a general expression for the amplitudes can be found in reference.⁷⁰ Thus, water exchange in general results in a multiexponential relaxation process, and estimation of CA concentration is not straightforward.

Obviously, a CA confined in a compartment of a multicompartiment system can become more or less invisible, unless a fast water exchange exists between all compartments, and the lack of fast exchange complicates estimation of the overall tissue concentration.

However, these problems can be ameliorated by the observation of Hazlewood that the initial slope of the MR signal relaxation curve is the same for the no-exchange and the fast-exchange regime.⁷⁸ This observation was taken up and elaborated further by Schwickert et al.⁷⁹ and Donahue et al.⁷⁶ Selecting appropriate MR imaging parameters can minimize the effect of the water exchange, so that the obtained MR signal becomes water exchange insensitive. An example is a two-compartment system, with no or slow water exchange, with the signal equation corresponding to a saturation recovery sequence:

$$S = S_0 v^a (1 - e^{-TD R_1^a}) + S_0 v^b (1 - e^{-TD R_1^b})$$

If TD is set to a low value, so that the exponential argument is below 0.2, then

$$S \approx S_0 TD (v^a R_1^a + v^b R_1^b) \approx S_0 (1 - e^{-TD(v^a R_1^a + v^b R_1^b)})$$

which is the signal one will obtain in case of a fast-exchange regime. Thus, the MR signal does not depend on details of the water exchange, and the effect is minimized for a low value of TD or TI. For a conventional GRE sequence (Eq. (41)), it is easy to show that

$$\frac{\cos \alpha}{1 - \cos \alpha} \frac{TR}{T_1} \ll 1 \quad (53)$$

will minimize the effect of water exchange,⁷⁶ that is, selecting a short TR and a relative high flip angle. The reason is that there is only a short time for manifestation of the evolution of the water exchange for short TR, TD, or TI, and the no-exchange model and the fast-exchange model will give the same result.

As previously mentioned, the water exchange between plasma and erythrocyte is believed to be very fast with a residence lifetime of about 10 to 15 milliseconds for a water molecule within the intracellular compartment.^{80,81} The water exchange between the capillary blood space and the extravascular extracellular space has been estimated to be less than 7 Hz, corresponding a mean lifetime of 140 milliseconds.^{72,76} If we assume no leakage between the vascular space and the extravascular space and a peak concentration of about 4 mM in the vascular space, and that the R_1 is roughly the same for tissue and blood before CA injection, then the difference in relaxation rates between the two compartments is about 16 Hz at the peak concentration. This should be compared with a water exchange rate of about 7 Hz. Obviously, even though we have a fast-exchange regime between compartments without any CA, we will enter an intermediate and slow water exchange regime during the bolus passage, and there is therefore a risk of underestimating the CA concentration, if we still assume a fast exchange. The largest CA segregation between the vascular space and the extravascular space is in the brain, due to the BBB, which is nearly impermeable for typical MR CA. In agreement with this, the cerebral perfusion was found to be eight times smaller for a TI = 0.9 seconds compared to TI = 20 milliseconds, but simulations showed only a 10% underestimation, if TI = 100 milliseconds. This is compatible with a water exchange rate of about 3 Hz between the vascular space and the extravascular space in human brain tissue.⁷⁰ Thus, the water exchange has a significant impact on DCE T_1 -weighted MRI in the brain, and water exchange minimization methods should be employed if the aim is perfusion measurement. This is also most likely for other organs if a macrocontrast agent molecule is used. In an in vivo animal study, Bjørnerud et al.⁸² studied the relaxation process in the heart using an intravascular CA and found evidence for a biexponential relaxation process with a water exchange rate between the vascular and extravascular space of 1.39 ± 0.52 Hz.

A more controversial issue is whether the interstitial water space is in fast-exchange regime with the intracellular water, for example, between the interstitial space and myocytes in the heart. Several studies have evaluated the water exchange between the interstitial space and the myocytes using isolated heart preparations. Wedeking et al.⁸³ found a cellular interstitial water exchange rate of 21 Hz in rat hearts and that fast exchange dominates as long as the interstitial CA concentration was below 1 mM. Donahue et al.⁷⁶ measured exchange rates of 8 to 27 Hz for the heart. Judd also studied both polylysine-Gd-DTPA and gadoteridol's effect on the water exchange regime in a heart preparation and found evidence for a slow water exchange regime for both compounds, but most pronounced for the intravascular polylysine-Gd-DTPA.⁸⁴ Vascular peak concentrations for polylysine-Gd-DTPD and gadoteridol were up to 15 and 25 mM, respectively, concentration which in our experience are far too high and never observed in humans, using conventional doses. Sobol et al.⁸⁵ showed that fast exchange existed up to an interstitial Gd-DTPA concentration of 10 mM in rat muscle. As seen, there is no general agreement about the level of cellular interstitial water exchange, and a large variation of the reported exchange rates is apparent. The exchange rate in some of these ex vivo studies could have been underestimated if carried out at a temperature of 20°C instead of 37°C, where water diffusion is higher. The concentration of CA in the interstitial space is related to the extraction fraction of the CA, and the interstitial concentration is usually lower than the plasma concentration. Own tracer kinetic modeling using a typical AIF with a peak concentration of 4 mM, a perfusion of 100 mL/100 g/min, and 50% extraction never results in a interstitial tissue concentration of more than 0.5 mM. In a further simulation study, the MR signal curves were very similar for fast, intermediate, and slow water exchange when extraction fractions were larger than 30% and for inversion times up to 800 milliseconds.⁷⁰ When extraction fraction was below 20%, the MR signal curves were clearly separated for fast and slow water exchange, when using a TI of 400 milliseconds or longer, but were similar when using a TI of 20 milliseconds. Thus, a high extraction fraction of a CA promotes conditions for a fast-exchange regime between the vascular and extravascular space, while an extraction fraction of zero, as occurs in the brain or when using macromolecular CA, tends to result in a slow water exchange condition between the vascular and extravascular space. Furthermore, it was also shown that a slow water exchange regime prevails when using an unphysiologic high arterial concentration (a factor 15), which cannot be compensated when using short inversion times (TI = 20 milliseconds). An in vivo human study showed equal myocardial perfusion values, regardless the value of TI in the interval 15 to 598 milliseconds.⁸⁶ This finding suggests that for the myocardium, the error of assuming fast water exchange both regarding the vascular and extravascular exchange and the cellular interstitial exchange are relatively small, and thus fast water exchange is likely a valid assumption in the heart. This is in contrast to the study of Landis et al.⁸⁷ In this study, the cellular interstitial water exchange was only fast up to an interstitial concentration of 0.1 mM. This suggests that it will be problematic to estimate extravascular tissue concentration in most situations, but the finding is not compatible with some of the previously mentioned results. Lately, Landis et al. study was contradicted by a study of human internal obturator muscle by Buckley et al.⁸⁸ In this study, only minimal difference was found when fitting a fast water exchange and a no-water exchange model to data, and the physiologic constants obtained were not dependent of the model of the water exchange being used. In addition, data suggested that a fast water exchange regime could be assumed for an interstitial concentration up to 0.5 mM. Finally, the study also pointed out the large uncertainty of estimated water exchange rates, making definite conclusion elusive. No doubt more elaborated models and measurements of the water exchange in various types of tissue are needed.⁸⁹ Generally, water exchange minimization methods are recommended.

Conclusion

Dynamic contrast-enhanced T₁-weighted MRI has the ability to provide important physiologic information. Compared with other methods, it is relatively simple to implement and integrate DCE-MRI in a standard MRI protocol. The advantages compared to dynamic susceptibility T₂*-weighted MRI is less susceptibility to field inhomogeneity, more reliable estimation of perfusion, and BBB permeability due to a robust relationship between concentration and longitudinal relaxation rate. Disadvantages are less coverage and a less favorable contrast to noise of tissue during the bolus passage. Implementation of fast multiband sequences will probably improve coverage, and higher field strength, for example, 7 T, might improve contrast to noise and also pave the way for direct estimation of water permeability in conjunction with estimation of other physiologic parameters.

REFERENCES

- Ballabh P, Braun A, Nedergaard M. The blood-brain barrier: an overview. Structure, regulation, and clinical implications. *Neurobiol Dis* 2004;16:1–13.
- Erickson MA, Banks WA. Blood-brain barrier dysfunction as a cause and consequence of Alzheimer's disease. *J Cereb Blood Flow Metab* 2013;33:1500–1513.
- Renkin EM. Transport of potassium-42 from blood to tissue in isolated mammalian skeletal muscles. *Am J Physiol* 1959;197:1205–1210.
- Crone C. The permeability of capillaries in various organs determined by use of the indicator diffusion method. *Acta Physiol Scand* 1963;58:292–305.
- Diesbourg LD, Prato FS, Wisenberg G, et al. Quantification of myocardial blood flow and extracellular volumes using a bolus injection of Gd-DTPA: kinetic modelling in canine ischemic disease. *Magn Reson Med* 1992;23(2):239–253.
- Larsson HB, Stubgaard M, Søndergaard L, et al. In vivo quantification of the unidirectional influx constant for Gd-DTPA diffusion across the myocardial capillaries with MR imaging. *J Magn Reson Imaging* 1994;4(3):433–440.
- Larsson HBW, Hansen AE, Berg HK, et al. Dynamic contrast-enhanced quantitative perfusion measurement of the brain using T₁-weighted MRI at 3 T. *J Magn Reson Imaging* 2008;27:754–762.
- Sourbron S, Ingrisch M, Siefert A, et al. Quantification of cerebral blood flow, cerebral blood volume, and blood-brain-barrier leakage with DCE-MRI. *Magn Reson Med* 2009;62:205–217.
- Kety SS, Schmidt CF. The nitrous oxide method for the quantitative determination of cerebral blood flow in man: theory, procedures and normal values. *J Clin Invest* 1948;27(4):476–483.
- Kety SS. The theory and applications of the exchange of inert gas at the lungs and tissues. *Pharmacol Rev* 1951;3(1):1–41.
- Meier P, Zierler KL. On the theory of the indicator-dilution method for measurement of blood flow and volume. *J Appl Physiol* 1954;6(12):731–744.
- Kuschinsky W, Paulson OB. Capillary circulation in the brain. *Cerebrovasc Brain Metab Rev* 1992;4(3):261–286.
- Jespersen SN, Østergaard L. The roles of cerebral blood flow, capillary transit time heterogeneity, and oxygen tension in brain oxygenation and metabolism. *J Cereb Blood Flow Metab* 2012;32:264–277.
- Fick A. Über die Messung des Blutquantums in den Herzventrikeln. *Sitzungsber. Physik Med Gesell zu Wurzburg* 1870;16:36.
- Lassen NA. Cerebral transit of an intravascular tracer may allow measurement of regional blood volume but not regional blood flow. *J Cereb Blood Flow Metab* 1984;4:633–634.
- Weisskoff RM, Chesler D, Boxerman JL, et al. Pitfalls in MR measurement of tissue blood flow with intravascular tracers: which mean transit time? *Magn Reson Med* 1993;29:553–559.
- Larsson HBW, Courivaud F, Rostrup E, et al. Measurement of brain perfusion, blood volume, and blood-brain barrier permeability, using dynamic contrast-enhanced T₁-weighted MRI at 3 tesla. *Magn Reson Med* 2009;62:1270–1281.
- Brix G, Semmler W, Port R, et al. Pharmacokinetic parameters in CNS Gd-DTPA enhanced MR imaging. *J Comput Assist Tomogr* 1991;15(4):621–628.
- Larsson HB, Stubgaard M, Frederiksen JL, et al. Quantitation of blood-brain barrier defect by magnetic resonance imaging and gadolinium-DTPA in patients with multiple sclerosis and brain tumors. *Magn Reson Med* 1990;16(1):117–131.
- Tofts PS, Kermode AG. Measurement of the blood-brain barrier permeability and leakage space using dynamic MR imaging. 1. Fundamental concepts. *Magn Reson Med* 1991;17(2):357–367.
- Larsson HBW, Fritz-Hansen T, Rostrup E, et al. Myocardial perfusion modelling using MRI. *Magn Reson Med* 1996;35:716–726.
- Tofts PS, Brix G, Buckley DL, et al. Estimating kinetic parameters from dynamic contrast-enhanced T₁-weighted MRI of a diffusible tracer: standardized quantities and symbols. *J Magn Reson Imaging* 1999;10:223–232.
- Cramer SP, Larsson HBW. Accurate determination of blood-brain barrier permeability using dynamic contrast enhanced T₁-weighted MRI. A simulation and in vivo study on healthy subjects and MS patients. *J Cereb Blood Flow Metab* 2014;34(10):1655–1665.
- Sourbron PS, Buckley DL. On the scope and interpretation of the Tofts models for DCE-MRI. *Magn Reson Med* 2011;66:735–745.
- Patlak CS, Blasberg RG. Graphical evaluation of the blood-to-brain transfer constants from multiple-time uptake data. Generalizations. *J Cereb Blood Flow Metab* 1985;5:584–590.
- Zwick S, Brix G, Tofts PS, et al. Simulation-based comparison of two approaches frequently used for dynamic contrast-enhanced MRI. *Eur Radiol* 2010;20:432–442.
- Cramer SP, Simonsen H, Frederiksen JL, et al. Abnormal blood-brain barrier permeability in normal appearing white matter in multiple sclerosis investigated by MRI. *Neuroimage Clin* 2014;4:182–189.
- Sangren WC, Sheppard CW. Mathematical derivation of the exchange of a labelled substance between a liquid flowing in a vessel and an external compartment. *Bull Math Biophys* 1953;15:387–394.
- Goresky CA, Ziegler WH, Bach GG. Capillary exchange modeling. Barrier-limited and flow limited distribution. *Circ Res* 1970;27:739–764.
- Koh TS, Bisdas S, Koh DM, et al. Fundamentals of tracer kinetics for dynamic contrast-enhanced MRI. *J Magn Reson Imaging* 2011;34:1262–1276.
- Koh TS, Tan CKM, Cheong LHD, et al. Cerebral perfusion mapping using a robust and efficient method for deconvolution analysis of dynamic contrast-enhanced images. *Neuroimage* 2006;32:643–653.
- Moran GR, Thornhill RE, Sykes J, et al. Myocardial viability imaging using Gd-DTPA: physiological modelling of infarcted myocardium, and impact on injection strategy and imaging time. *Magn Reson Med* 2002;48:791–800.
- Koh TS, Thng CH, Hartono S, et al. Dynamic contrast-enhanced MRI of neuroendocrine hepatic metastases: a feasibility study using a dual-input two-compartment model. *Magn Reson Med* 2011;65:250–260.
- Johnson JA, Wilson TA. A model for capillary exchange. *Am J Physiol* 1966;210(6):1299–1303.
- St. Lawrence KS, Lee TY. An adiabatic approximation to the tissue homogeneity model for water exchange in the brain: I. Theoretical derivation. *J Cereb Blood Flow Metab* 1998;18(12):1365–1377.
- St. Lawrence KS, Lee TY. An adiabatic approximation to the tissue homogeneity model for water exchange in the brain: II. Experimental validation. *J Cereb Blood Flow Metab* 1998;18(12):1378–1385.
- Bassingthwaigthe JB, Goresky CA. Modeling in the analysis of solute and water exchange in the microvasculature. In: Renkin EM, Michel CC, Geiger SR, eds. *Handbook of physiology. Section 2. The cardiovascular system*. Bethesda, MD: American Physiological Society; 1984:549–626.
- Bassingthwaigthe JB, Malone MA, Moffett TC, et al. Validity of microsphere depositions for regional myocardial flows. *Am J Physiol* 1987;253:H184–H193.
- Østergaard L, Weisskoff RM, Chesler DA, et al. High resolution measurement of cerebral blood flow using intravascular tracer bolus passages. Part I: Mathematical approach and statistical analysis. *Magn Reson Med* 1996;36:715–725.
- Tikhonov AN, Arsenin, eds. *Solutions of ill-posed problems*. John F, transl. editor. Washington, DC: V.H. Winston; 1977.
- Tikhonov AN. Ill-posed problems in natural sciences. In: Leonov AS, ed. *Proceedings of International Conference, Moscow*; 1991.
- Hansen PC. *Rank-deficient and ill-posed problems*. Doctoral Dissertation. UniC. Technical University of Denmark; 1996.
- Schmitt M, Viallon M, Thelen M, et al. Quantification of myocardial flow and blood flow reserve in the presence of arterial dispersion: a simulation study. *Magn Reson Med* 2002;47:787–793.

44. Calamante F, Gadian DG, Connelly A. Delay and dispersion effects in dynamic susceptibility contrast MRI: Simulations using singular value decomposition. *Magn Reson Med* 2000;44:466–473.
45. Elkinington AG, He T, Gatehouse PD, et al. Optimization of the arterial input function for myocardial perfusion cardiovascular magnetic resonance. *J Magn Reson Imaging* 2005;21:354–359.
46. Boos M, Scheffler K, Haselhorst R, et al. Arterial first pass gadolinium-CM dynamics as a function of several intravenous saline flush and Gd volumes. *J Magn Reson Imaging* 2001;13:568–576.
47. Van Osch MJP, Vonken EPA, Wu O, et al. Model of the human vasculature for studying the influence of contrast injection speed on cerebral perfusion MRI. *Magn Reson Med* 2003;50:614–622.
48. Fritz-Hansen T, Rostrop E, Larsson HBW, et al. Measurement of the arterial concentration of Gd-DTPA using MRI: a step toward quantitative perfusion imaging. *Magn Reson Med* 1996;36:225–231.
49. Hansen A, Pedersen H, Rostrop E, et al. Partial volume effect (PVE) on the arterial input function (AIF) in T_1 -weighted perfusion imaging and limitations of the multiplicative rescaling approach. *Magn Reson Med* 2009;62:1055–1059.
50. Van Osch MJP, Vonken EPA, Bakker CJG, et al. Correcting partial volume artifacts of the arterial input function in quantitative cerebral perfusion MRI. *Magn Reson Med* 2001;45:477–485.
51. Conturo TE, Barker PB, Mathews VP, et al. MR imaging of cerebral perfusion by phase-angle reconstruction of bolus paramagnetic-induced frequency shift. *Magn Reson Med* 1992;27(2):375–390.
52. Gatehouse PD, Elkinington AG, Ablitt NA, et al. Accurate assessment of the arterial input function during high-dose myocardial perfusion cardiovascular magnetic resonance. *J Magn Reson Imaging* 2004;20:39–45.
53. Kleppetø M, Larsson C, Groote I, et al. T_2^* -correction in dynamic contrast-enhanced MRI from double-echo acquisitions. *J Magn Reson Imaging* 2014;39:1314–1319.
54. Christian TF, Rettmann DW, Aletras AH, et al. Absolute myocardial perfusion in canines measured by using dual-bolus first-pass MR imaging. *Radiology* 2004;232:677–684.
55. Hsu LY, Rhoads KL, Holly JE, et al. Quantitative myocardial perfusion analysis with a dual-bolus contrast-enhanced first-pass MRI technique in humans. *J Magn Reson Imaging* 2006;23:315–322.
56. Köstler H, Ritter C, Lipp M, et al. Prebolus quantitative MR heart perfusion imaging. *Magn Reson Med* 2004;52:296–299.
57. Kim D, Axel L. Multislice, dual-imaging sequence for increasing the dynamic range of the contrast-enhanced blood signal and CNR of myocardial enhancement at 3T. *J Magn Reson Imaging* 2006;23:81–86.
58. Yang C, Karczmar GS, Medved M, et al. Multiple reference tissue method for contrast agent arterial input function estimation. *Magn Reson Med* 2007;58:1266–1275.
59. Yang C, Karczmar GS, Medved M, et al. Reproducibility assessment of a multiple reference tissue method for quantitative dynamic contrast enhanced-MRI analysis. *Magn Reson Med* 2009;61:851–859.
60. Fluckiger JU, Schabel MC, DiBella EVR. Model-based blind estimation of kinetic parameters in DCE-MRI. *Magn Reson Med* 2009;62(6):1477–1486.
61. Schabel MC, Fluckiger JU, DiBella EVR. A model-constrained Monte Carlo method for blind arterial input function estimation in dynamic contrast-enhanced MRI: I) simulations. *Phys Med Biol* 2010;55(16):4783–4806.
62. Calamante F, Willats LW, Gadian DG, et al. Bolus delay and dispersion in perfusion MRI: implications for tissue predictor models in stroke. *Magn Reson Med* 2006;55:1180–1185.
63. Schabel MC, DiBella EVR, Jensen RL, et al. A model-constrained Monte Carlo method for blind arterial input function estimation in dynamic contrast-enhanced MRI: I) in vivo results. *Phys Med Biol* 2010;55(16):4807–4823.
64. Calamante F, Mørup M, Hansen LK. Defining a local arterial input function for perfusion MRI using independent component analysis. *Magn Reson Med* 2004;52:789–797.
65. Gadian DG, Payne JA, Bryant DJ, et al. Gadolinium-DTPA as a contrast agent in MR imaging—theoretical projections and practical observations. *J Comput Assist Tomogr* 1985;9(2):242–251.
66. Lauffer RB. Paramagnetic metal complexes as water proton relaxation agents for NMR imaging: theory and design. *Chem Rev* 1987;87:901–927.
67. Donahue KM, Burstein D, Manning WJ, et al. Studies of Gd-DTPA relaxivity and proton exchange rates in tissue. *Magn Reson Med* 1994;32:66–76.
68. Fintaske J, Martirosian P, Graf H, et al. Relaxivity of Gadopentetate Dimeglumina (Magnevist), Gadobutrol (Gadovist), and Gadobenate Dimeglumine (MultiHance) in human blood plasma and 0.2, 1.5 and 3 tesla. *Invest Radiol* 2006;41:213–221.
69. Heye T, Boll DT, Reiner C, et al. Impact of precontrast T_{10} relaxation times on dynamic contrast-enhanced MRI pharmacokinetic parameters: T_{10} mapping versus a fixed T_{10} reference value. *J Magn Reson Imaging* 2014;39:1136–1145.
70. Larsson HBW, Rosenbaum S, Fritz-Hansen T. Quantification of the effect of water exchange in dynamic contrast MRI perfusion measurements in the brain and heart. *Magn Reson Med* 2001;46:272–281.
71. Brix G, Schad LR, Deimling M, et al. Fast and precise T_1 imaging using tomrop sequence. *Magn Reson Imaging* 1990;8:351–356.
72. McLaughlin A, Leigh J. Relaxation times in systems with chemical exchange: approximate solutions for the non dilute case. *J Magn Reson* 1973;9:296–304.
73. Donahue KM, Weisskoff RM, Burstein D. Water diffusion and exchange as they influence contrast enhancement. *J Magn Reson Imaging* 1997;7:102–110.
74. Colon T, Outhred R. Water diffusion permeability of erythrocytes using an NMR technique. *Biochim Biophys Acta* 1972;288:354–361.
75. Koenig SH, Spiller M, Brown RD, et al. Relaxation of water protons in the intra- and extracellular regions of blood containing Gd(DTPA). *Magn Reson Med* 1986;3:791–795.
76. Donahue KM, Weisskoff RM, Chesler DA, et al. Improving MR quantification of regional blood volume with intravascular T_1 contrast agent: accuracy, precision, and water exchange. *Magn Reson Med* 1996;36:858–867.
77. Zimmerman JR, Brittin WE. Nuclear magnetic resonance studies in multiple phase systems: lifetime of a water molecule in an adsorbing phase on silica gel. *J Phys Chem* 1957;61:1328–1333.
78. Hazlewood C, Chang D, Nichols B, et al. Nuclear magnetic resonance transverse relaxation times of water protons in skeletal muscle. *Biophys J* 1974;14:583–605.
79. Schwickert HC, Roberts TP, Shames DM. Quantification of liver blood volume: comparison of ultra short T_1 inversion recovery echo planar imaging (ULSTAR-EPI), with dynamic 3D-gradient recalled echo imaging. *Magn Reson Med* 1995;34:845–852.
80. Fabry ME, Eisenstadt M. Water exchange between red cells and plasma. Measurement by nuclear magnetic relaxation. *Biophys J* 1975;15(1):1101–1110.
81. Bruno E, Digilio G, Cabella C, et al. Water exchange across the erythrocyte plasma membrane studied by HR-MAS NMR spectroscopy. *Magn Reson Med* 2006;56(5):978–985.
82. Bjørnerud A, Bjerner T, Johansson LO, et al. Assessment of myocardial blood volume and water exchange: theoretical considerations and in vivo results. *Magn Reson Med* 2003;49:828–837.
83. Wedeking P, Sotak CH, Telsler J, et al. Quantitative dependence of MR signal intensity on tissue concentration of Gd(HP-DO3A) in nephrectomized rat. *Magn Reson Imaging* 1992;10:97–108.
84. Judd RM, Atalay MK, Rottman GA, et al. Effects of myocardial water exchange on T_1 enhancement during bolus administration of MR contrast agents. *Magn Reson Med* 1995;33:215–223.
85. Sobol WT, Jackels SC, Cothran RL, et al. NMR spin-lattice relaxation in tissues with high concentration of paramagnetic contrast media: evaluation of water exchange rates in intact rat muscle. *Med Phys* 1991;18:243–250.
86. Nielsen G, Fritz-Hansen T, Dirks CG, et al. Evaluation of heart perfusion in patients with acute myocardial infarction using dynamic contrast-enhanced magnetic resonance imaging. *J Magn Reson Imaging* 2004;20:403–410.
87. Landis CS, Li X, Telang FW, et al. Equilibrium transcytolemmal water-exchange kinetics in skeletal muscle in vivo. *Magn Reson Med* 1999;4:467–478.
88. Buckley DL, Kershaw LE, Stanisz GJ. Cellular-interstitial water exchange and its effect on the determination of contrast agent concentration in vivo: dynamic contrast-enhanced MRI of human internal obturator muscle. *Magn Reson Med* 2008;60:1011–1019.
89. Moran GR, Prato FS. Modeling (1H) exchange: an estimated of the error introduced in MRI by assuming the fast exchange limit in bolus tracking. *Magn Reson Med* 2004;51(4):816–827.